5105-136
Solar Thermal Power Systems Project
Parabolic Dish Systems Development

DOE/JPL-1060-74
Distribution Category UC-62

A Nomographic Methodology for Use in Performance Trade-Off Studies of Parabolic Dish Solar Power Modules

M.K. Selçuk
T. Fujita

June 15, 1984

Prepared for
U.S. Department of Energy
Through an Agreement with
National Aeronautics and Space Administration
by
Jet Propulsion Laboratory
California Institute of Technology
Pasadena, California

JPL Publication 84-39

5105-136
Solar Thermal Power Systems Project
Parabolic Dish Systems Development

DOE/JPL-1060-74
Distribution Category UC-62

A Nomographic Methodology for Use in Performance Trade-Off Studies of Parabolic Dish Solar Power Modules

M.K. Selçuk
T. Fujita

June 15, 1984

Prepared for
U.S. Department of Energy
Through an Agreement with
National Aeronautics and Space Administration
by
Jet Propulsion Laboratory
California Institute of Technology
Pasadena, California

JPL Publication 84-39

Prepared by the Jet Propulsion Laboratory, California Institute of Technology, for the U.S. Department of Energy through an agreement with the National Aeronautics and Space Administration.

The JPL Solar Thermal Power Systems Project is sponsored by the U.S. Department of Energy and is part of the Solar Thermal Program to develop low-cost solar thermal and electric power plants.

ABSTRACT

A simple graphical method has been developed to undertake technical design trade-off studies for individual parabolic dish modules comprising a two-axis tracking parabolic dish with a cavity receiver and power conversion assembly at the focal point. The results of these technical studies can then be used in performing the techno-economic analyses required for determining appropriate subsystem sizing. Selected graphs that characterize the performance of subsystems within the module have been arranged in the form of a nomogram that would enable an investigator to carry out several design trade-off studies. Key performance parameters encompassed in the nomogram include receiver losses, intercept factor, engine rating, and engine efficiency. Design and operation parameters such as concentrator size, receiver type (open or windowed aperture), receiver aperture size, operating temperature of the receiver and engine, engine partial load characteristics, concentrator slope error, and the type of reflector surface, are also included in the graphical solution. Cost considerations are not included.

The nomogram has been used to perform trade-off studies that have provided a basis for determining requirements for a single concentrator that could perform satisfactorily with either the selected Stirling or Brayton engine. This activity is summarized to illustrate the usage of the nomogram.

Additionally, modeling relations used in developing the nomogram are presented so that the nomogram can be updated to reflect any changes in the performance characteristics of projected components.

PREFACE

The nomogram was developed specifically to encompass modules employing advanced kinematic Stirling or Brayton engines coupled with either open or windowed cavity receivers. The Stirling engine is an advanced version of the Model 4-95 engine developed by United Stirling AB, while the Brayton is predicated upon the use of a solar version of the automotive Advanced Gas Turbine (AGT) being developed by the Garrett Turbine Engine Company.

ACKNOWLEDGEMENTS

The authors wish to express their gratitude to Dr. E. John Roschke for his useful recommendations and critique of the manuscript, to Maxine Koop for typing the text, and Peggy Panda for editorial assistance.

The work described herein was conducted by the Jet Propulsion Laboratory, California Institute of Technology, for the U.S. Department of Energy through an agreement with the National Aeronautics and Space Administration (NASA Task RE-152, Amendment 327; DOE/ALO/NASA Interagency Agreement No. DE-AM04-80AL13137).

NOMENCLATURE

A	area
CR	concentration ratio
D	diameter
f	concentrator focal length
G	geometric shading factor
h_r	radiative heat transfer coefficient
h_c	convective heat loss coefficient
h_k	conductance of the insulated receiver wall
I	insolation
J	focal plane flux intensity
Q	maximum collectible heat
R	radius
T	temperature
W	power output of the engine

Greek Symbols

α	effective absorptance of the cavity receiver
ε	effective emittance of the cavity receiver
ϕ	intercept factor
η	efficiency
σ_s	surface errors for the concentrator
σ_t	tracking errors for the concentrator
ρ	reflectance of the mirror surface
τ	transmittance
θ	divergence of the reflected beam

Subscripts

a	receiver aperture
alt	alternator
b	beam
c	concentrator
con	concentrator
eng	engine
in	input
L	loss
m	projected mirror, equivalent to concentrator
o	optical
out	output
rec	receiver
rw	receiver wall
sys	system
u	unit area
w	window

CONTENTS

Figures

SECTION I

INTRODUCTION

This report presents a nomographic methodology for conducting technical design trade-off studies for parabolic dish systems. As shown in Figure 1-1, the dish is composed of a point-focusing concentrator having two-axis tracking and a receiver/engine assembly mounted at the focal point.

A. BACKGROUND

The performance characteristics of parabolic dish concentrators and cavity-type receivers have been analyzed by several investigators at the Jet Propulsion Laboratory (JPL) (Refs. 1 through 4). Additional design and test experience was gained through projects managed at JPL. These activities include the development of an air Brayton solar receiver (ABSR) (Ref. 5), a ceramic honeycomb-type receiver with a quartz window (Ref. 6), a steam receiver (Ref. 7) and an organic-fluid (toluene) receiver (Ref. 8). Testing of these receivers was conducted at the Parabolic Dish Test Site at Edwards Air Force Base in California. Test data on the performance of the Stirling receiver alone are not available. Because the heater head of the Stirling engine is an integral part of the receiver, the engine and receiver were tested as a complete assembly.

The studies cited above and several others (e.g., Refs. 9 through 14) examined many aspects of the design and performance prediction for the concentrator and receiver. These studies provide the basis for developing a nomogram to undertake, in a rapid manner, design trade-off studies and to determine the sensitivity of the module performance to variations in subsystem performance characteristics.

Because numerous users exist for performing rapid trade-off studies, a nomogram to facilitate these studies was developed. This nomogram was used in conducting trade-off studies to provide requirements data for a Program Opportunity Notice (PON) concerned with design, fabrication, and test of advanced concentrators.

The PON was aimed at developing advanced solar power generation modules. The best current estimates of the characteristics of advanced power assemblies were needed to determine the specifications for the concentrators.

The nomogram developed to serve this need was utilized to examine modules employing advanced kinematic Stirling and Brayton engines coupled with either open or windowed cavity receivers. To show how the nomogram is used, results are presented of the trade-off studies directed toward providing a basis for determining requirements for a single concentrator that could perform satisfactorily with either the selected Stirling or Brayton engine.

This report contains mathematical relations and the bases for formulating the thermal performance of the components of the parabolic dish power module so that the nomogram can be updated to reflect any changes in the projected component characteristics.

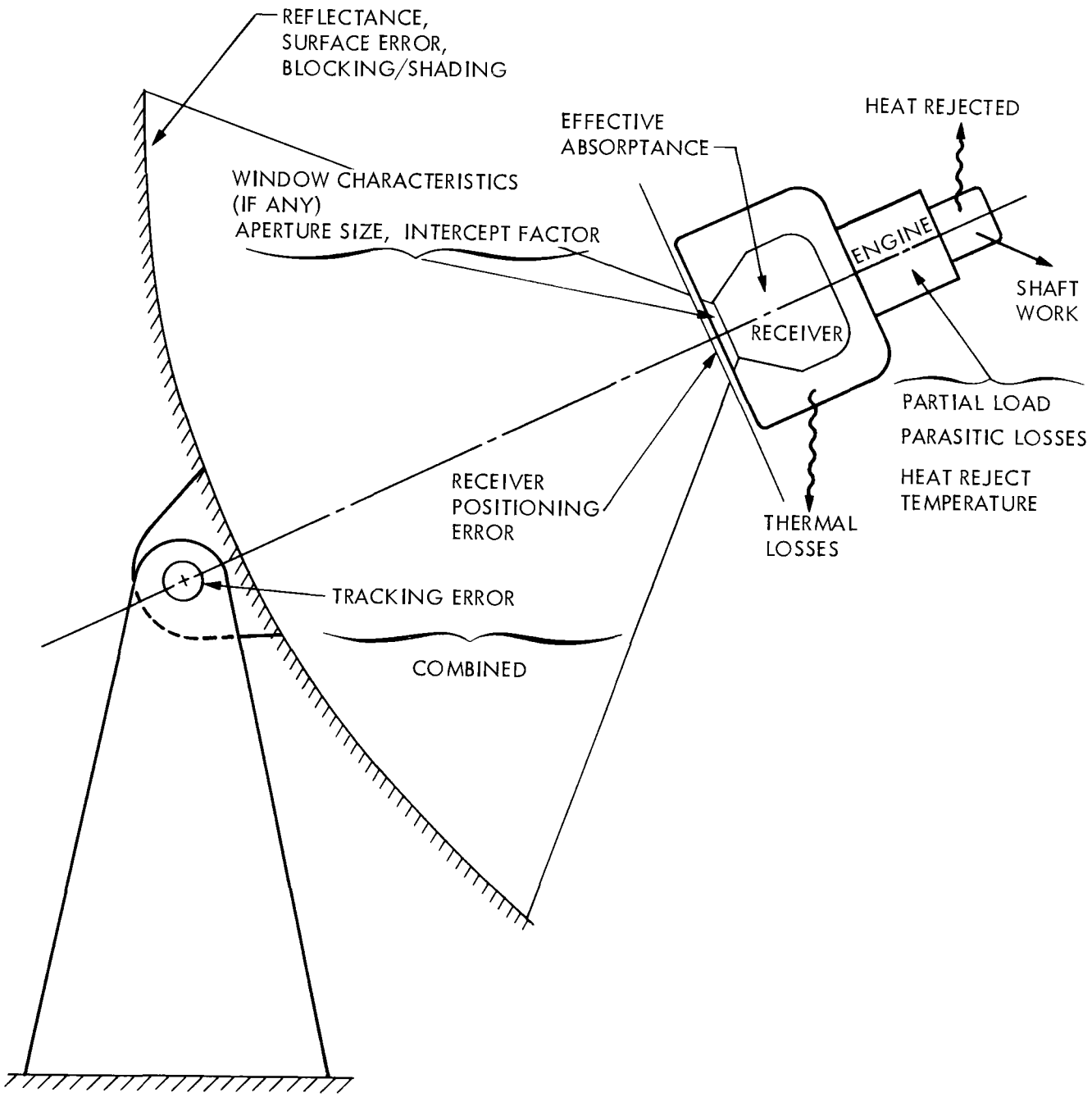

Figure 1-1. Parabolic Dish Power Module Components and Design and Operational Factors

B. OBJECTIVES

The objectives of the study are to develop a nomographic methodology that

(1) Permits a rapid but reasonably accurate determination of component and system performance for use in performance/cost trade-off studies.

(2) Enables the rapid assessment of sensitivities associated with uncertainties in projecting the characteristics of the advanced power assemblies.

(3) Provides a straightforward means of deriving performance specifications for advanced concentrators that are to be developed for use with advanced receiver/engine/generator power assemblies.

C. SCOPE AND APPROACH

In undertaking the study, detailed analytical models with exhaustive computer usage have been avoided. Instead, simple but reasonably accurate mathematical models of the receiver performance were developed as the basis for a nomographic solution methodology. Results of earlier analyses predicting the optical performance of the concentrator and conversion efficiencies of Stirling and Brayton engines were also used in developing the nomogram.

The nomogram was developed by incorporating the results of several analyses. Graphical representation of the performances of the concentrator, the receiver, and the engine are assembled to form a multi-part nomogram to enable the user to visualize the interrelations of the performance of each component with other components, and the effects of variations in design and operational parameters.

Obviously, the nomogram is not meant to generate results of high accuracy, but does yield results generally better than 10%.

SECTION II

DESCRIPTION OF THE METHODOLOGY

A. DESCRIPTION OF THE NOMOGRAM AND ITS COMPONENTS

Figure 1-1 (page 1-2) depicts the components of the solar parabolic dish power conversion module and indicates the parameters that affect the performance of each component. Detailed discussion of the interrelations of these parameters are presented in the following sections.

Design and operational parameters related to module performance and indicated in Figure 1-1 are grouped below:

(1) Parameters related to concentrator performance

- (a) Reflectance.
- (b) Mirror slope error.
- (c) Concentrator tracking error.
- (d) Receiver and supporting structure shading.

(2) Parameters related to receiver performance

- (a) Aperture size.
- (b) Effective absorptance of the cavity surface.
- (c) Receiver positioning error (usually combined with mirror errors).
- (d) The intercept factor (related to mirror geometry and surface slope errors).
- (e) Thermal losses.

(3) Parameters related to engine performance

- (a) Engine cycle efficiency and mechanical efficiency.
- (b) Part-load characteristics.
- (c) Heat rejection.
- (d) Parasitic losses.

These parameters are used in analyzing module performance by means of a nomogram; Figure 2-1 shows the components of the nomogram. The nomogram consists of three portions: (1) concentrator, (2) receiver, and (3) engine. Each portion of the nomogram can be used individually to determine the approximate performance of a module subsystem when the required input data is supplied.

A general description of the nomogram presented in Figure 2-2 is provided below in terms of the treatment of each major portion.

1. Concentrator

The treatment of the circular concentrator requires the following inputs:

(a) Concentrator area (projected mirror area) : A_c

(b) Concentrator mirror diameter : D_m

(c) Concentrator focal length : f

(d) Reflector material reflectance : ρ

(e) Tracking and surface errors for the concentrator : (σ_t, σ_s)

(f) Shading factor : G

This information enables one to determine the total concentrated flux in the vicinity of the focal plane from the relation

$$Q = A_c I_b G \rho \qquad (1)$$

where I_b = insolation in kW/m^2

G = shading factor

ρ = reflectance.

Note that Q is the maximum amount of heat collectible, and that this amount of heat can be collected only if the receiver aperture has captured the entire concentrated flux without spillage and if the effective absorptance (α) is unity. In actuality, some part of the concentrated flux is spilled because of a factor of ϕ, which is called the intercept factor, and the effective cavity absorptance is less than unity.

To minimize reradiation losses from the aperture of the cavity receiver, a small aperture is desired. In practice, minimum overall heat losses correspond to an aperture that is sized to allow a small amount of spillage. Additionally, there are other spillage losses caused by receiver positioning errors associated with the tracking and control system and by wind-induced vibrations. These errors are combined with the tracking error and are incorporated in the term ϕ.

If the effects of spillage and effective absorptance are included, the net heat delivered by the concentrator to the receiver becomes

$$Q_c = A_c I_b G \rho \phi \alpha \qquad (2)$$

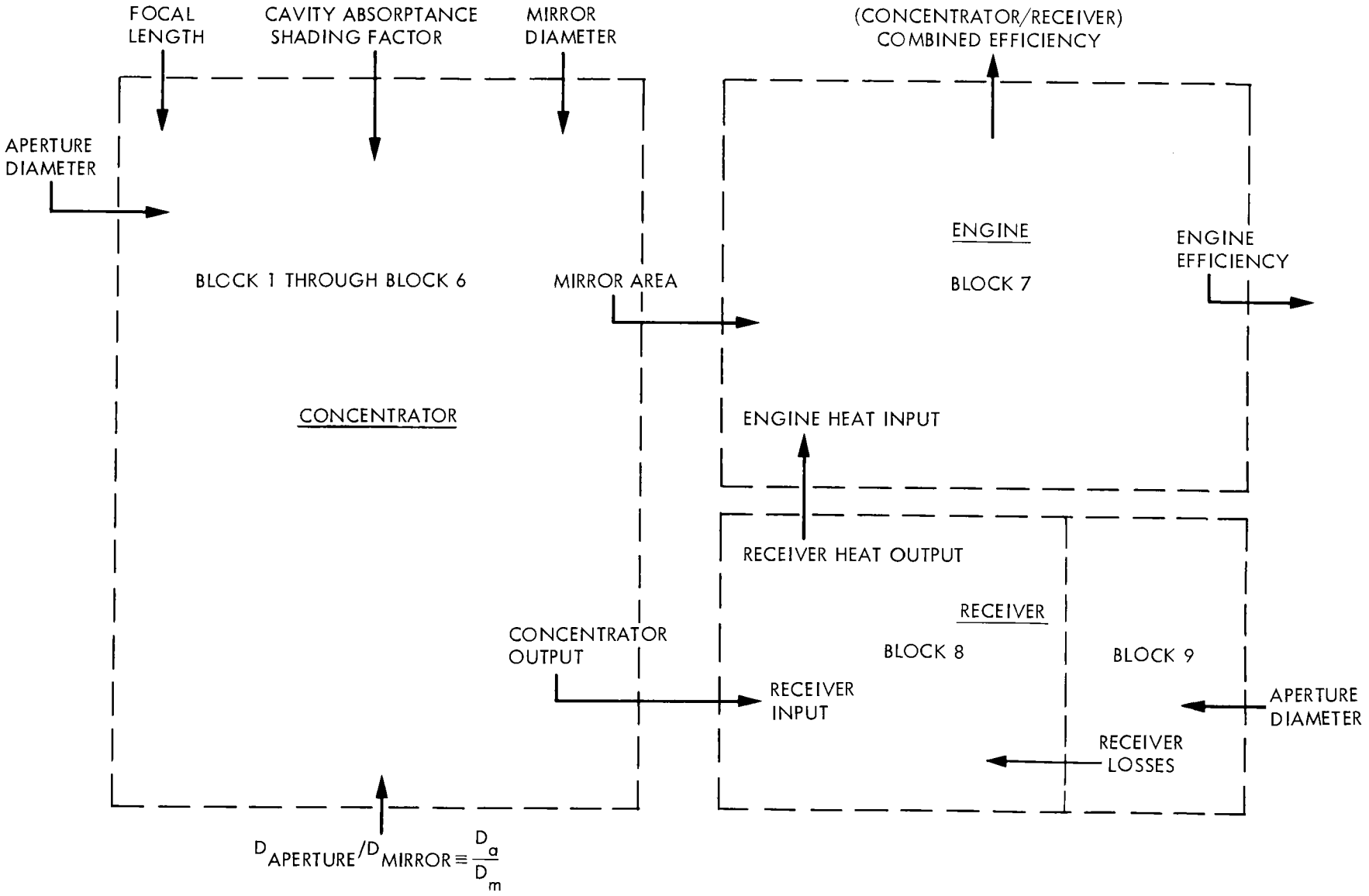

Figure 2-1. Components of the Nomogram

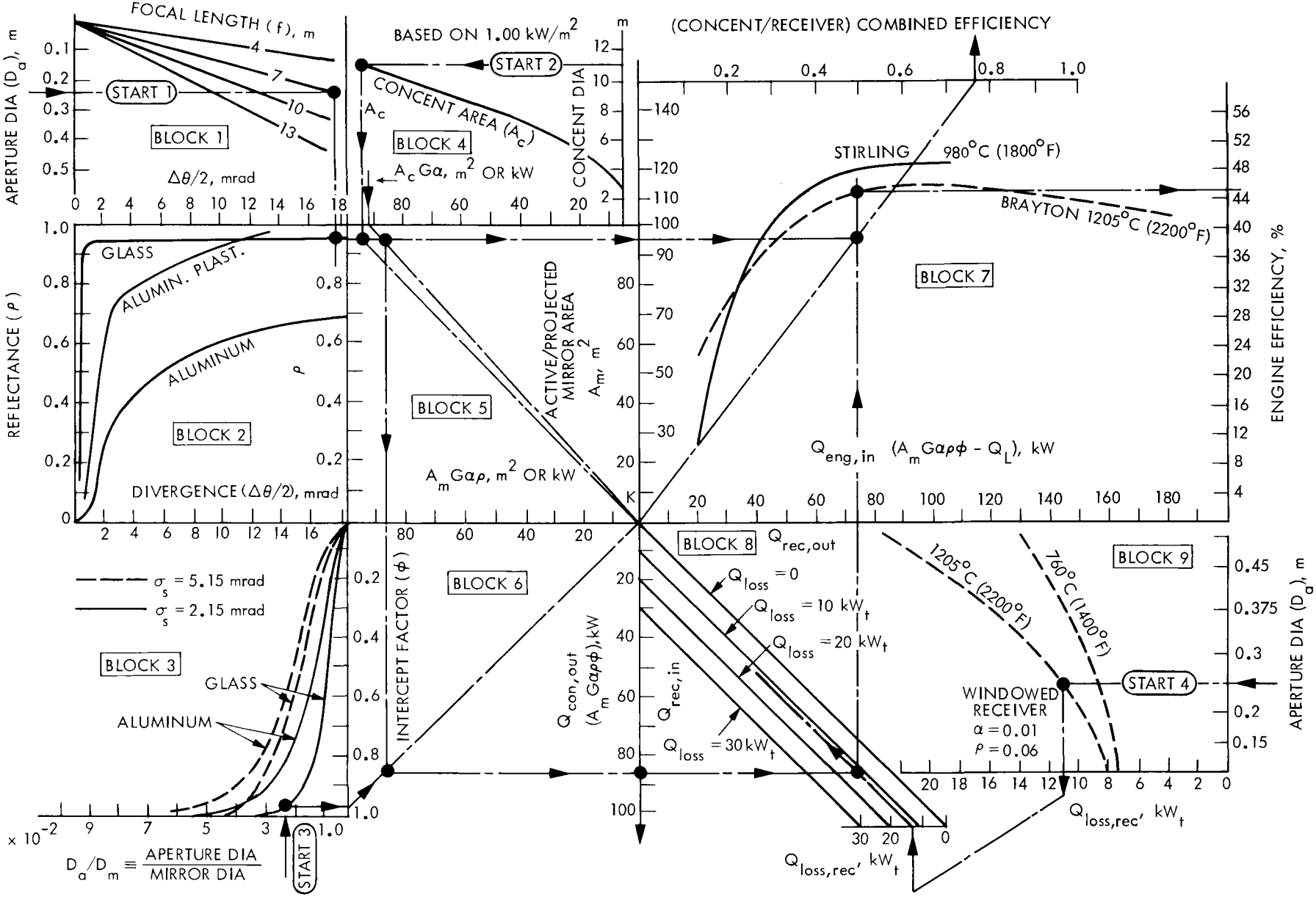

Figure 2-2. Parabolic Dish Optimization Nomogram
(See center of report for enlargement)

2. Receiver

The receiver portion of the nomogram yields the net heat output of the receiver for a given heat input and aperture size. The nomogram covers receivers that have either open cavities or cavities with windowed apertures. The receiver portion of the nomogram is entered with the amount of heat supplied by the concentrator, operating temperature, and receiver aperture. The resulting output is the net heat delivered to the engine. It should be noted that due to the wide range of operating temperatures and variations in the properties of materials used, in practice, several curves relating heat loss and aperture size could be developed. However, it was found that a single curve could be used to give results within reasonable error. Because use of such a single curve is advantageous in simplifying the nomogram, it has been adopted for the methodology presented in this report. Later sections will present further details that show the impact of this simplification.

3. Engine

The final step of the performance evaluation of a parabolic dish power module is to determine the shaft output of the engine. The engine portion of the nomogram provides this output for selected Brayton and Stirling engines as a function of the heat supplied by the receiver. Thus, if the engine portion of the nomogram is entered with the output of the receiver portion, both the engine efficiency and the shaft power are obtained. The nomogram shown in Figure 2-2 displays engine efficiency curves for a single temperature level. Additional curves for other temperature values will be supplied in a later section of this report.

The characteristics of the selected Brayton engine are based on the expected performance of a solar version of the automotive Advanced Gas Turbine (AGT) being developed by the Garrett Turbine Engine Company. The selected Stirling engine has performance characteristics conforming with projections of an advanced version of the 4-95 engine being developed by United Stirling AB of Sweden (USAB). At the present time, both of these engines are candidates for advanced parabolic dish power systems.

B. INTERACTIONS AMONG THE COMPONENTS OF THE NOMOGRAM

The interactions among the components can be visualized by following the flow of energy from the sun to the concentrator, receiver, and engine in a sequential manner. The factors that govern the processing or flow of energy within each component and the interface where energy is transferred from one component to another are all contained within the nomogram. A convenient way of demonstrating these interactions is to consider a parabolic dish module having a specified design. When the nomogram is used to determine the power output and efficiency of the module, one can see how each parameter used in specifying the design is employed in the nomogram.

The following example for a fixed design shows the interactions within the nomogram. The selected design is specified by the following parameters:

D_m = 11-m mirror diameter

f = 7-m focal length

D_a = 0.25-m aperture diameter (windowed receiver)

α_w = 0.01 window absorptance

ρ_w = 0.06 window reflectance

I_b = 1000 W/m^2 insolation

G = 0.98 shading factor

Mirror: Corning Glass 0317

σ_s = 2.15 mrad (1/8-deg) surface and pointing errors

T_{rec} = 1205°C (2200°F)

Engine: Brayton 1205°C (2200°F)

The solution procedure as illustrated in Figure 2-2 involves the following steps. To find the reflectance of the mirror surface corresponding to the beam divergence $\Delta\theta/2$, and focal length of f:

Enter at START 1: D_a = 0.25 m; intersect f = 7 m (BLOCK 1)

Read: ρ = 0.95 reflectance for Corning Glass 0317 (BLOCK 2)

: $\Delta\theta/2$ = 17.8 mrad divergence of the reflected beam (BLOCK 2)

Enter at START 2: D_m = 11 m (BLOCK 4)

Read: A_m = 95 m^2 -- the gross mirror area

Follow the vertical line at A_m = 95 m^2 until it intersects the 45-deg line in BLOCK 5, then proceed horizontally and carry the A_m value to the engine portion of the nomogram for later use in BLOCK 7. Corrections may be required for cavity absorptance, α, which is about 0.99 and shading factor, G, which is about 0.99. Thus, the $G\alpha$ product is about 0.98. With shadow and absorptance losses, the net area becomes:

$$A_m G\alpha = 95 \times 0.98 = 93 \text{ m}^2 \quad (3)$$

For 1.000 kW/m^2 insolation the result also gives the energy value in thermal kilowatts (kW$_t$)

$$A_m G\alpha I_b = 93 \text{ kW}_t \quad (4)$$

Please note that the arrow indicating $A_m G\alpha$ = 93 m^2 in BLOCK 4 is shifted from the A_m = 95 m^2 arrow.

In BLOCK 3, enter at START 3: (D_a/D_m) x 100 = 2.27 and σ_s = 2.15 mrad for glass. Read ϕ = 0.98 intercept factor.

Follow the horizontal line at ρ = 0.95 in BLOCK 2 and intersect with the slanted dashed line in BLOCK 5 that joins $A_m G\alpha$ = 93 m^2 arrow tip and the origin K of BLOCKs 5, 6, 7, and 8. The intersection gives $A_m G\alpha\rho$ = 88 m^2 in BLOCK 5. In BLOCK 6, join ϕ = 0.98 arrow tip with the origin K and intersect this line with $A_m G\alpha\rho$ = 88 m^2 line.

Read the $Q_{con,out}$ on the right-hand-side scale of BLOCK 6 for 1000 W/m^2, $A_m G\alpha\rho$ = 86 m^2 and $I_b A_m G\alpha\rho\phi$ = 86 kW_t. $I_b A_m G\alpha\rho\phi$ = 86 kW_t is the concentrator output that is entered into BLOCK 8 as receiver input.

Note that for insolation levels other than 1000 W/m^2, a correction to $Q_{rec,in}$ must be applied. Then

$$Q_{rec,in,I_b} = Q_{rec,in} \times \frac{I}{1000} \qquad (5)$$

In BLOCK 9, enter at START 4, using D_a = 0.25 m (10 in.).

Receiver heat losses = 11 kW_t = Q_L for a windowed receiver at 1205°C (2200°F).

Full size Q_L versus aperture curves are presented in Figure 2-3.

Intersect $Q_{rec,in}$ = 86 kW_t and slanted Q_L = 11 kW line.

On the upper scale of BLOCK 8, read: $Q_{rec,out} = Q_{eng,in}$ = 74 kW_t.

In BLOCK 7 enter on the left-hand scale at 95 m^2 and lower scale $Q_{eng,in}$ = 74 kW_t.

The intersection point of these lines is joined with the origin K and extended to the upper scale where the concentrator/receiver combined efficiency = 0.78 is obtained.

A_m can be entered directly on the vertical A_m scale in BLOCK 5 or carried from horizontal scale by intersecting the continuation of START 2 line which flows vertically down.

It should be noted that the overlap of ρ = 0.95 and A_m = 95 m^2 values is coincidental!

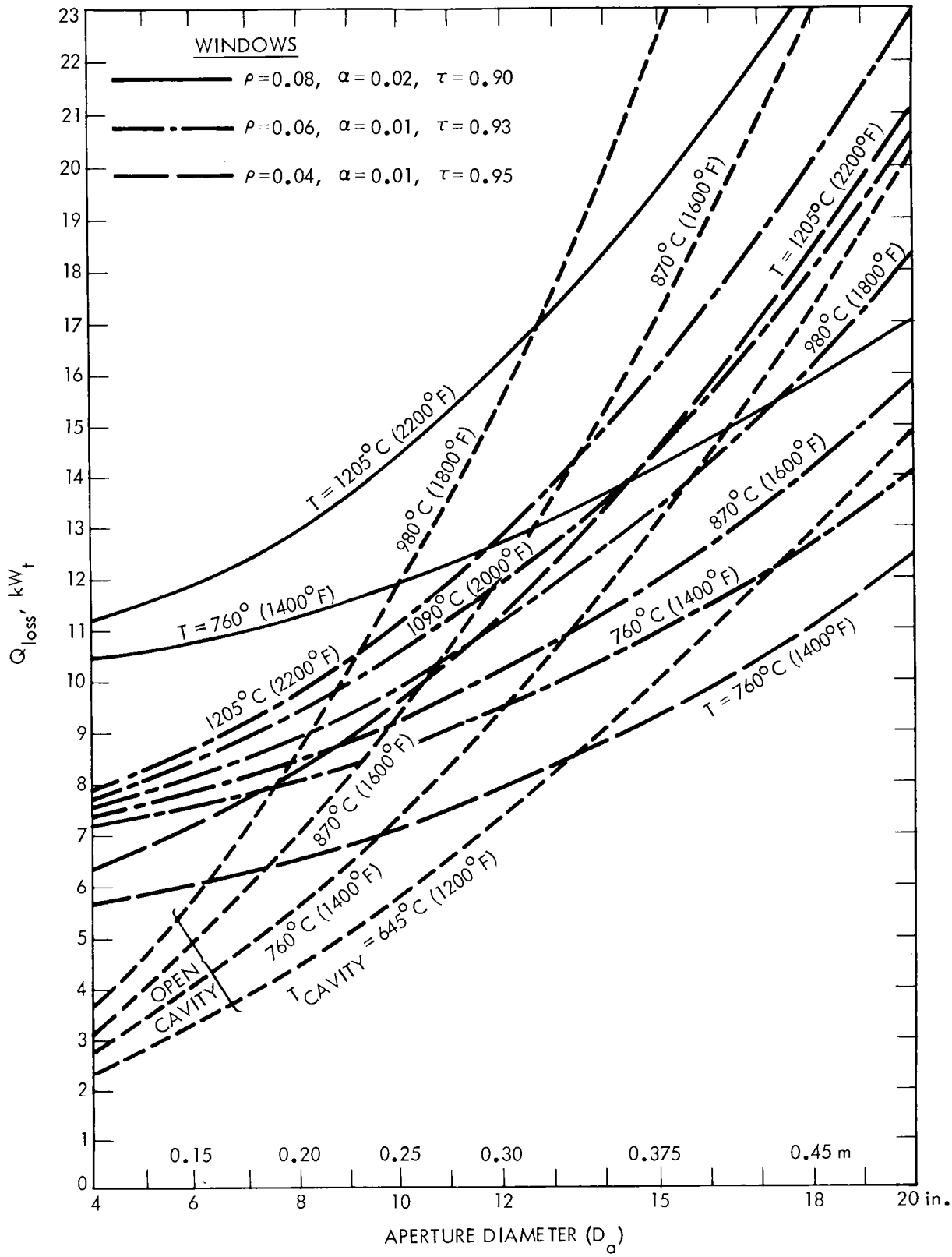

Figure 2-3. Heat Loss Curves for Open Cavity and Windowed Receivers

Entering: $Q_{eng,in}$ = 74 kW_t and intersecting Brayton 1205°C (2200°F) curve,

Read: η_{eng} = 0.45.

The shaft work output of the engine can be calculated by multiplying the heat input and the engine efficiency:

$$W_{out} = 74 \times 0.45 = 33.3\ kW_{shaft} \quad (6)$$

If an alternator is coupled to the engine shaft, the net electricity generation should then be calculated from

$$E = W_{out} \cdot \eta_{alt} \quad (7)$$

where E = electricity generated in kW_e

η_{alt} = alternator efficiency.

NOTE: The best, intermediate, and worst windows have transmittances of 0.95, 0.93, and 0.90, respectively.

SECTION III

APPLICATIONS OF THE NOMOGRAM

The nomogram of Figure 2-2 can be used to address numerous design trade-off issues. Two important uses are treated in this section. The first involves the use of the nomogram in system technical performance optimization; inherent in this application is the sensitivity of system performance to design parameters. Insights regarding dominant parameters and basic trends resulting from design perturbations are gleaned from this type of application.

The second application involves the use of the nomogram to determine performance requirements for a major system component subject to a set of constraints. A particular example is treated wherein the nomogram is used to determine performance requirements for an advanced concentrator.

A. OVERALL SYSTEM OPTIMIZATION

The general process employed in using the nomogram to optimize the performance of the system is first described. Then, some basic trends deduced from implementing the optimization procedure are presented.

1. Description of the Process

The graphical solution to the problem of module optimization may require several iterations before an approximate value is obtained. First, some of the key values such as the module size, required power output, and operation temperature limits have to be assumed. In some instances, a definite concentrator size or operation temperature may not be available. Under such circumstances, several values may be selected and module efficiencies for each case may be obtained; then, results are compared with each other to obtain the best solution.

Steps in optimizing module design and performance follow:

(1) Select basic concentrator design data. Some or all of the following data may be used:

   (a) Concentrator diameter and focal length.

   (b) Reflector material.

   (c) Mirror slope and tracking errors.

(2) Obtain net heat available at the focal plane of the concentrator using the component concentrator portion of the nomogram. A receiver aperture has to be assumed to determine the intercept factor, ϕ.

(3) Select receiver design data. The following basic information is needed for an accurate determination of receiver losses:

(a) Insulation material properties and thickness.

(b) Aperture size, which already has been assumed to determine the intercept factor.

(c) Optical properties of the absorbing surface (cavity).

(d) Optical properties of the transparent window, if any.

The present nomogram, however, simplifies this process, and approximate heat losses are determined as a function of receiver aperture and temperature only. For windowed receivers, heat loss curves for high and low transmittance window characteristics are given. The receiver portion of the nomogram yields the net heat out, which is used as the heat input to the engine.

(4) Determine engine efficiency, overall system efficiency, and shaft power output by using the engine portion of the nomogram.

This concludes the first iteration in predicting module performance. Additional iterations may be needed before a final design is achieved. The final optimization process involves the capital cost (including financing and and related tax implications) and operation and maintenance (O&M) expenses of the module and its components. The present study does not include any cost predictions. In order to select a design that produces the lowest cost per unit of useful heat, the technical subsystem specifications established by such a nomographic method must be iterated with module costing and economic analyses.

2. Basic Trends Deduced from Optimization/Sensitivity Studies

The most important design and operation parameters of parabolic dish modules as determined from optimization studies are grouped below under the three categories of (a) concentrator, (b) receiver, and (c) engine.

a. Concentrator. Concentrator performance is affected by the reflectance of the mirror surfaces and their specularity. The reflectance value used here is the directional reflectance value with a finite view angle. The receiver aperture, which captures the reflected beam, must be considered in defining the reflectance. Other important parameters are the slope errors, which are related to the design and fabrication of the mirror, and tracking errors, which are related to normal operation. Obviously, glass and similar highly specular surfaces yield intercept factors higher than that of polished aluminum. Particularly for small aperture mirror diameter ratios, i.e., high concentration ratios, the intercept factor is low. Reflectance, specularity of the mirror surfaces, slope and tracking errors, receiver losses for aperture sizes larger than 20 cm (8 in.), and engine operating temperatures are sensitive design parameters. Those parameters influencing the optimal design can be varied within some limits. Although a set of optimum design and operation parameters valid for most instances cannot be quoted, limits of these parameters can be suggested. For example, the concentrator diameter for a nearly optimal design appears to vary from 10 to 12 m for an engine assembly rated at 20 kW_e power. Although the Brayton engines available for solar power modules are capable of generating almost twice as much power as the Stirling engine, particularly USAB Model 4-95, this capacity

may not be used given the limitations of the concentrator. Although dishes larger than 12 m can be built, larger sizes tend to make the concentrator structural design difficult and increase the cost per unit area, whereas small sizes require increased number of engines and trackers for a given plant size. Outside the optimal concentrator size range, the efficiency of the module is reduced and the cost is increased.

The receiver aperture diameter and focal length of the concentrator should be selected such that the resulting divergence of the reflected beam lies above the knee of the reflectance curves. For glass, $\Delta\theta/2 > 5$ mrad is recommended, and for polished aluminum, $\Delta\theta/2 > 10$ mrad. Tolerable surface and pointing errors are less than 1/3 deg, i.e., 5.15 mrad. For such an error level, recommended maximum concentration ratios are about 2500 for glass mirrors, and 1600 for polished aluminum mirrors, respectively.

b. Receiver. Receiver performance is affected mainly by the aperture size and whether the aperture is open or has a window. Figure 2-3 shows heat loss as a function of aperture size for both cases at various cavity temperatures. For a receiver with windows, properties of the window material play an important role in the amount of heat lost.

Receiver losses are dominated by convection and radiation from the aperture for open cavity receivers. A reasonable range for aperture size is 0.15 to 0.25 m (6 to 10 in.) for the temperature levels under consideration, i.e., about 760 to 1205°C. For window receivers studied, receiver thermal losses of 12 kW_t or less are being recommended. For receivers with higher window absorptance, i.e., $\alpha_w = 0.02$, the aperture diameter varies from 0.19 to 0.25 m (7.5 to 10 in.) for 1205 and 760°C (2200 and 1400°F), respectively. Higher window transmittance or lower absorptance ($\alpha_w = 0.01$) allows larger aperture diameters, 0.32 to 0.48 m (12.5 to 19 in.), respectively. These values correspond to a nominal concentrator output/receiver input of 80 kW_t.

Increasing the aperture size increases the intercept factor, ϕ, which means that more heat is input into the receiver. This, however, increases the receiver thermal losses. It may become necessary to increase the aperture size to accept a major portion of the concentrated flux, particularly with concentrators having large surface and tracking errors and poor specularity. The selection of an aperture size that yields maximum receiver output is an example typical of useful trade-off studies.

c. Engines. Engine performance is influenced by the operation (cycle) temperature and its part-load characteristics. Sample part-load characteristics of Brayton and Stirling engines are presented in Figures 3-1 and 3-2, respectively. Obviously, the objective of the performance optimization studies is to maximize the engine power output for a given mirror size.

For practical energy generation purposes, lower limits for heat inputs are suggested to be about 20 kW_t for Brayton engines operating at 760°C (1400°F) and 1205°C (2200°F) and advanced (4-95) Stirling engines operating at 720°C (1328°F). At least 30 kW_t heat inputs are expected for 4-95 Stirling engines operating at 760 and 980°C (1400 and 1800°F), respectively. Engine performance is limited to a threshold heat input below which the engine cannot produce useful power output. This value ranges from 10 to 20 kW_t.

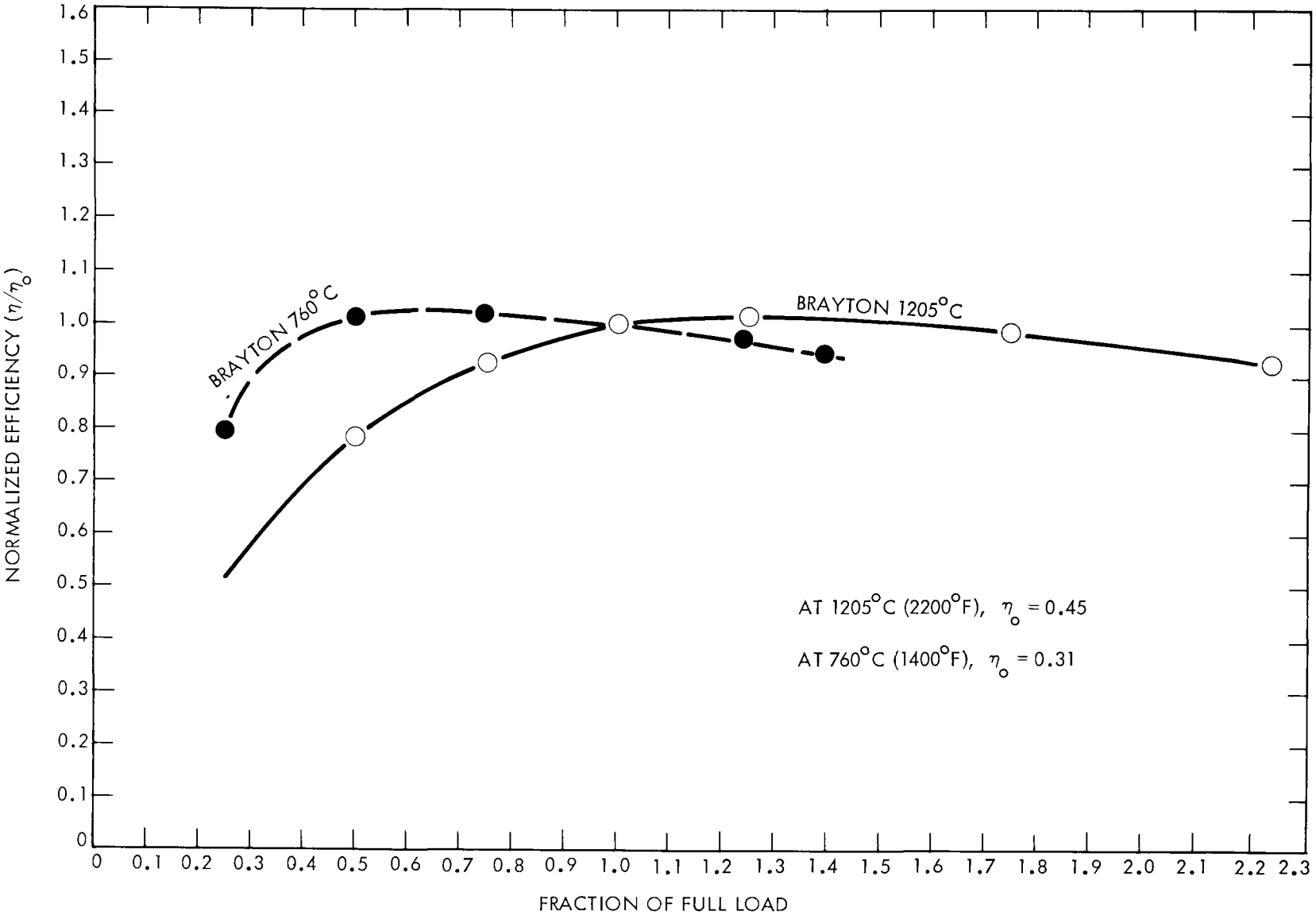

Figure 3-1. Brayton Engine Part-Load Characteristics

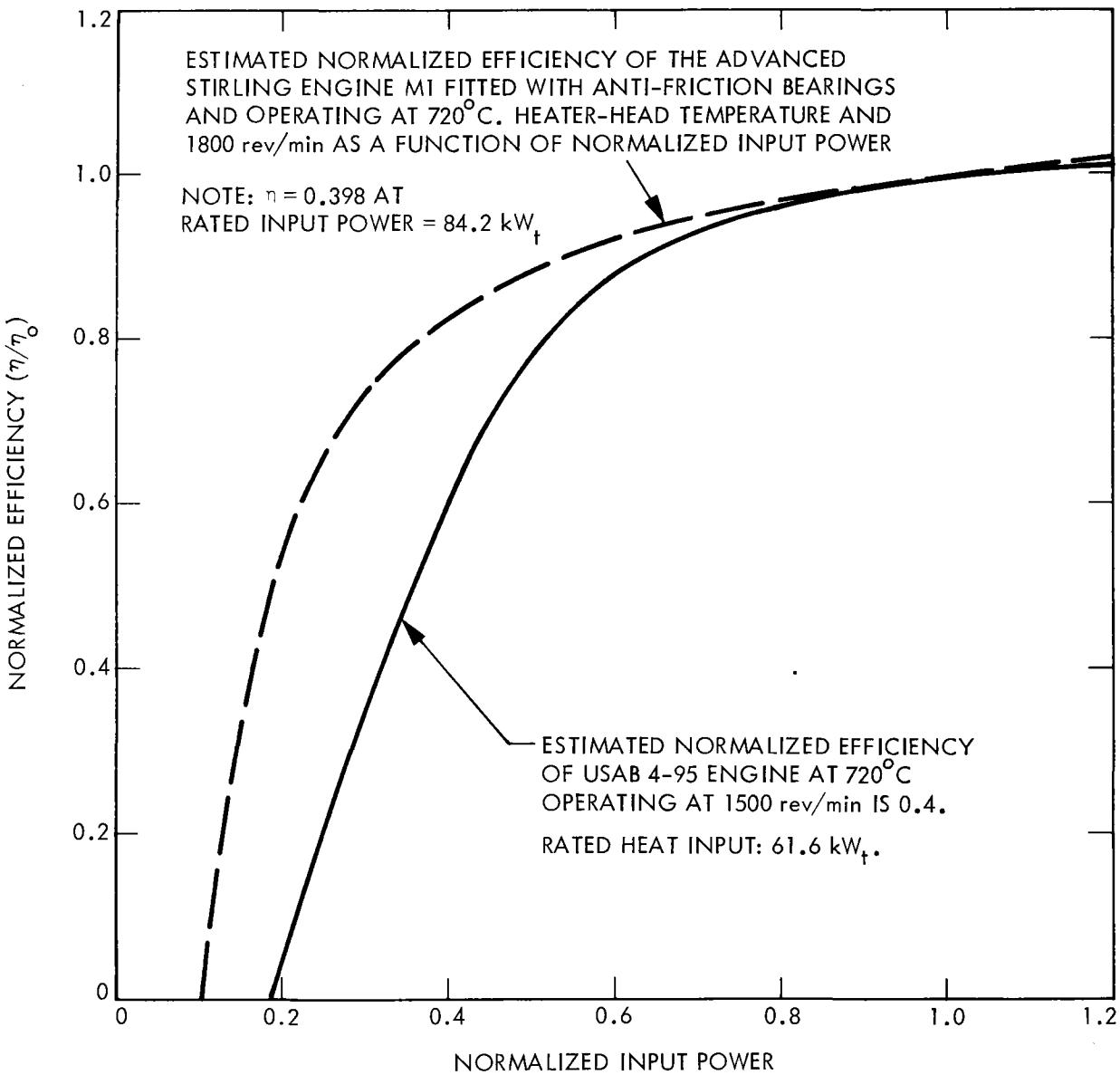

Figure 3-2. Stirling Engine Part-Load Curves

B. PERFORMANCE REQUIREMENTS FOR AN ADVANCED CONCENTRATOR

The nomogram was used to develop performance requirements for advanced concentrators suitable for use with projected advanced receiver/engine/generator power assemblies. Sensitivities associated with uncertainties in projecting characteristics of advanced power assemblies were also assessed.

1. Definition of the Problem

The problem for which the nomogram is used entailed developing the concentrator output requirements to match Brayton and Stirling power modules. Based on the thermal energy requirements of either module, relations of thermal power versus aperture need to be set. The concentrator design parameters are flexible as long as the final concentrator output satisfies the requirements set for the given aperture size. The studies are based on the projected size and weight characteristics of the power assemblies, as well as on performance requirements in terms of the flux that must enter the receiver (as a function of receiver aperture size) in order to supply the design power ratings. Also, sensitivity studies are conducted to determine (1) the effect of uncertainties on the specifications and (2) the impacts that could arise from mismatches between concentrators designed to meet the requirements and power assemblies that depart from projected characteristics used in developing the concentrator specifications.

2. Solution Using the Nomogram

Using the nomogram, steps in generating the performance requirements for advanced concentrators are presented below:

a. Selection of a Typical Heat Loss Curve for all Receivers. Because the advanced concentrator is required to supply reflected solar energy to both a Brayton engine with a windowed receiver and a Stirling engine with an open-cavity receiver, one curve was generated as the typical receiver loss curve. The reasons for selecting the engine and receiver types are the availability of a rather mature high-temperature ceramic matrix-type air heater with a quartz window for use in conjunction with Brayton engines up to 1205°C (2200°F) and successful tests with open-cavity Stirling receivers. This curve approximates the performance of both types of receivers identified earlier in Figure 2-3. Figure 3-3 is a curve of receiver heat loss versus aperture size selected for this purpose.

This curve should be considered a compromise between designing several concentrators and receivers that each serve a specific purpose or working with a single curve that approximates the receiver performance for a wide range of temperatures. For 80 kW_t, heat input errors involved in calculating the net receiver output, i.e., heat input minus losses, are about (10.25 - 14.5)/(80 - 14.5) x 100 = -6.5% if the receiver operates at about 650°C. Thus, for most of the practical designs, the error is less than 7%.

In general, this single curve is suitable for general trade-off studies involving either an open-cavity or a windowed receiver. If a well defined

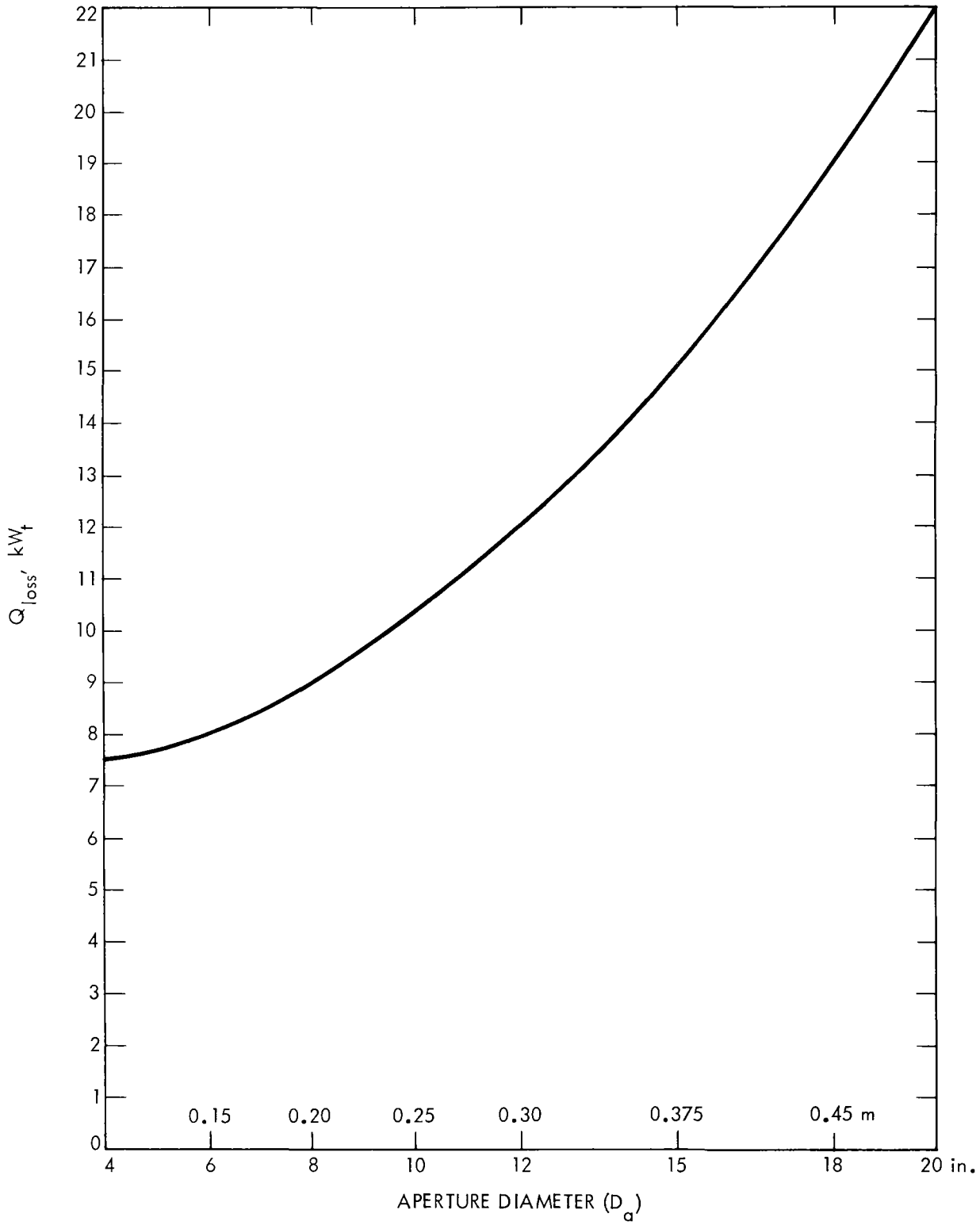

Figure 3-3. General Heat Losses versus Aperture Size

performance curve for a particular receiver is readily available, Figure 3-3 should be replaced with that specific curve. It should also be noted that material properties are temperature dependent, particularly with receiver windows to be used at high temperatures. Therefore, the heat loss values may deviate from those predicted in Figure 3-3. The nomogram presented (Figure 2-2) has a curve representing heat losses of a windowed receiver operating at 1205°C (2200°F) as specified in the case study. Heat loss values for other types of receivers and operating temperatures must be obtained from Figure 2-3 and carried to BLOCK 9 then to BLOCK 8 of the nomogram. Performance curves presented in the rest of this section are also based on Figure 3-3.

b. Performance of Engine/Receiver Combinations. Performances of both Brayton and Stirling engines are predicted using the nomogram presented and the single heat loss curve presented in Figure 3-3. Because the nominal heat required to operate either engine at its design point is fixed (80 kW_t for the examples presented), the concentrator should provide an amount equal to 80 kW_t plus receiver losses.

In this analysis, the concentrator heat supply $Q_{rec,in}$ is represented by a single curve. In Figure 3-4, there is a curve labeled $Q_{rec,in}$, which is common to both the Brayton and Stirling engine systems. Actual receiver losses, on the other hand, differ slightly because receiver characteristics vary with specific requirements.

Following are the performance predictions for Brayton and Stirling engines. The nomogram has been repeatedly used to generate the points used in plotting curves.

c. Brayton Engine/Receiver Performance. Figure 3-4 shows the variation of the input power required, $Q_{rec,in}$, as a function of aperture diameter. The required heat input varies from 87.5 to 102 kW_t for aperture sizes of 0.10 and 0.50 m (4 and 20 in.), respectively. The net heat available to the engine for conversion into shaft power is the difference between the heat input into the receiver, $Q_{in,rec}$, minus receiver losses. Figure 3-4 also gives the net heat supplied by the receiver for Brayton engines operating at turbine inlet temperatures of 1205 and 760°C (2200 and 1400°F). The Brayton receivers are windowed receivers because presently a functional and efficient ceramic receiver with a window capable of producing temperatures up to 1400°C is available.

The shaft power output of Brayton engines are plotted in Figure 3-5. The power output at 1205°C (2200°F) is almost independent of aperture size and is a high value of 36.4 kW_{shaft} out of a nominal engine heat input of 80 kW_t. At such high temperatures, increased aperture diameter barely compensates for the heat losses that increase with increasing aperture diameter. Therefore, the receiver net heat output and resulting Brayton engine heat output are almost constant.

On the other hand, at 760°C (1400°F), engine output increases with increasing aperture diameter because the rate of increase of heat loss is less than the increase of the net heat output of the receiver, which results in increased power output.

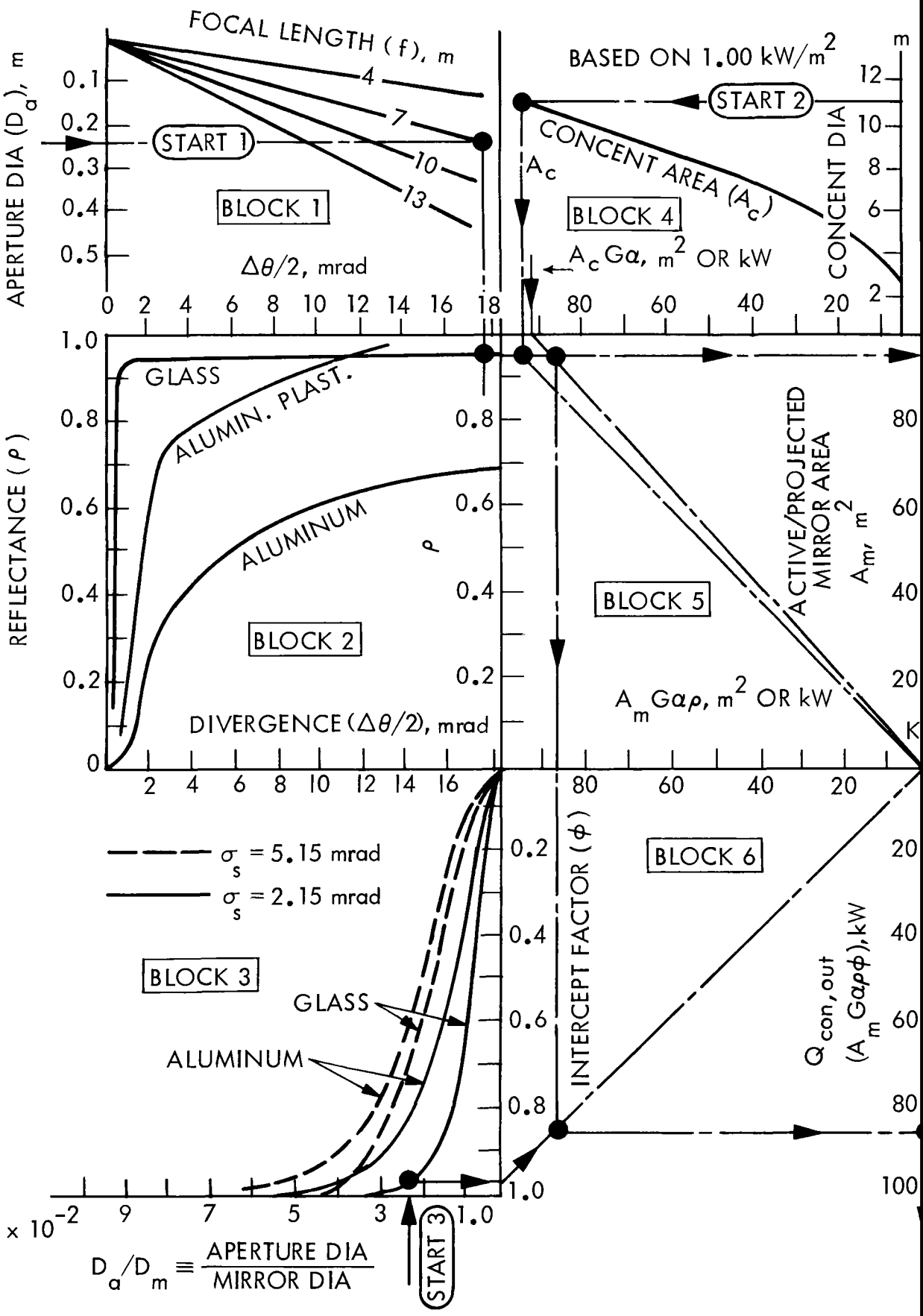
FOCAL LENGTH (f), m
4
7
10
13
APERTURE DIA (D_a), m
START 1
BLOCK 1
$\Delta\theta/2$, mrad
BASED ON 1.00 kW/m^2
START 2
CONCENT AREA (A_c)
CONCENT DIA
A_c
BLOCK 4
$A_c G\alpha$, m^2 OR kW
REFLECTANCE (ρ)
GLASS
ALUMIN. PLAST.
ALUMINUM
ρ
BLOCK 2
DIVERGENCE ($\Delta\theta/2$), mrad
BLOCK 5
ACTIVE/PROJECTED MIRROR AREA A_m, m^2
$A_m G\alpha\rho$, m^2 OR kW
σ_s = 5.15 mrad
σ_s = 2.15 mrad
BLOCK 3
GLASS
ALUMINUM
INTERCEPT FACTOR (ϕ)
BLOCK 6
$Q_{con,out}$ ($A_m G\alpha\rho\phi$), kW
x 10^{-2}
$D_a/D_m \equiv \frac{\text{APERTURE DIA}}{\text{MIRROR DIA}}$
START 3

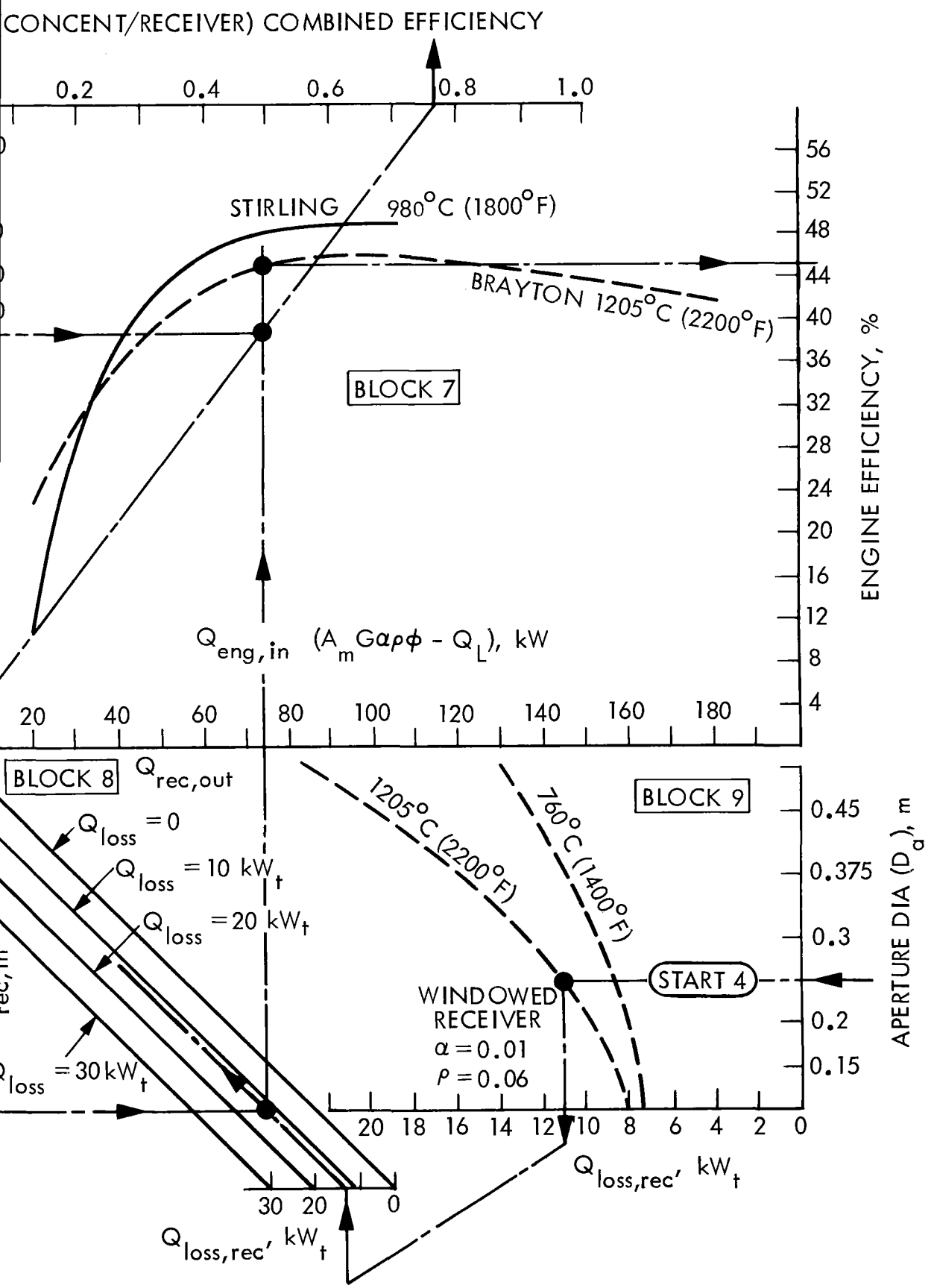

IZATION NOMOGRAM

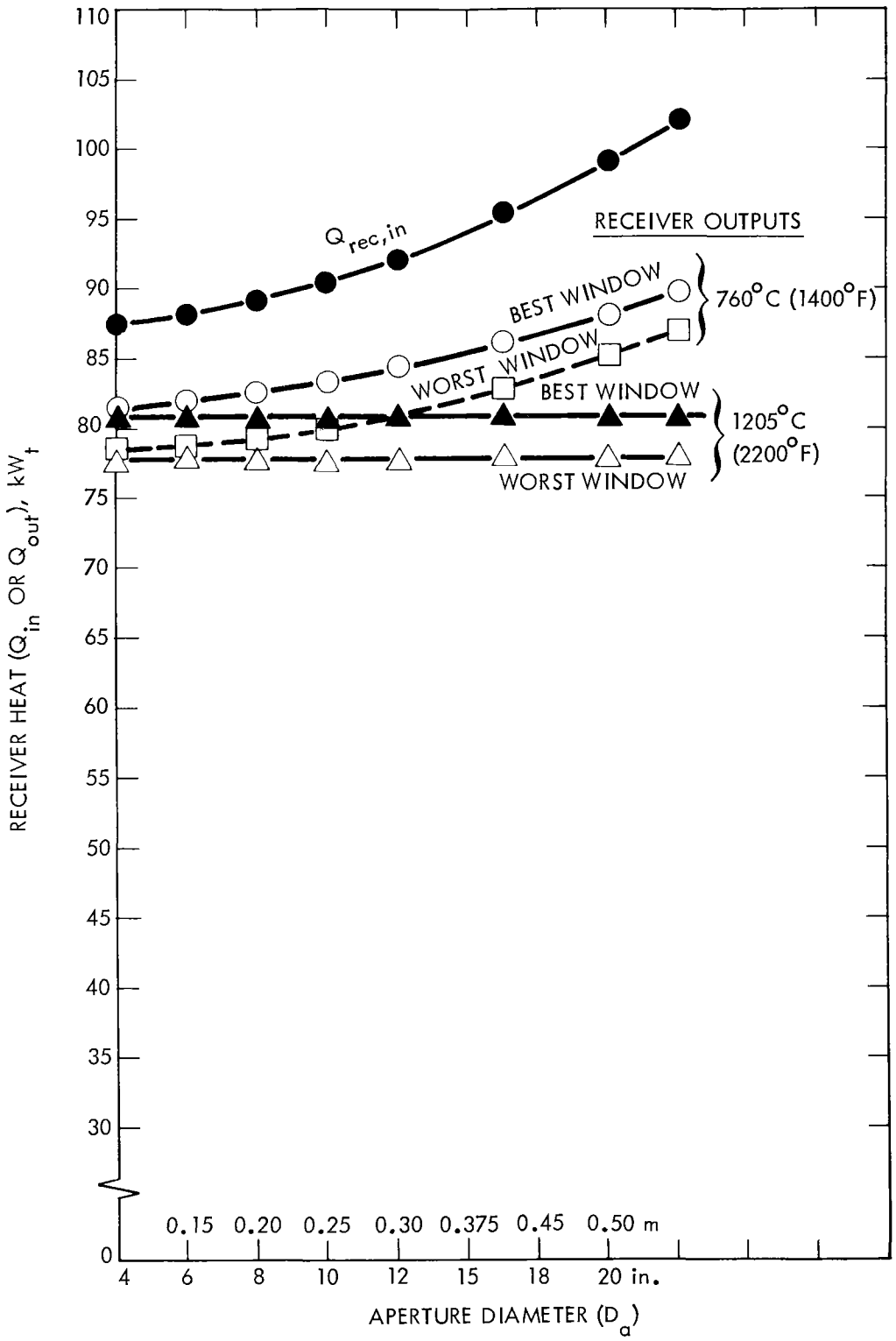

Figure 3-4. Receiver Heat Input/Output for Brayton Engines

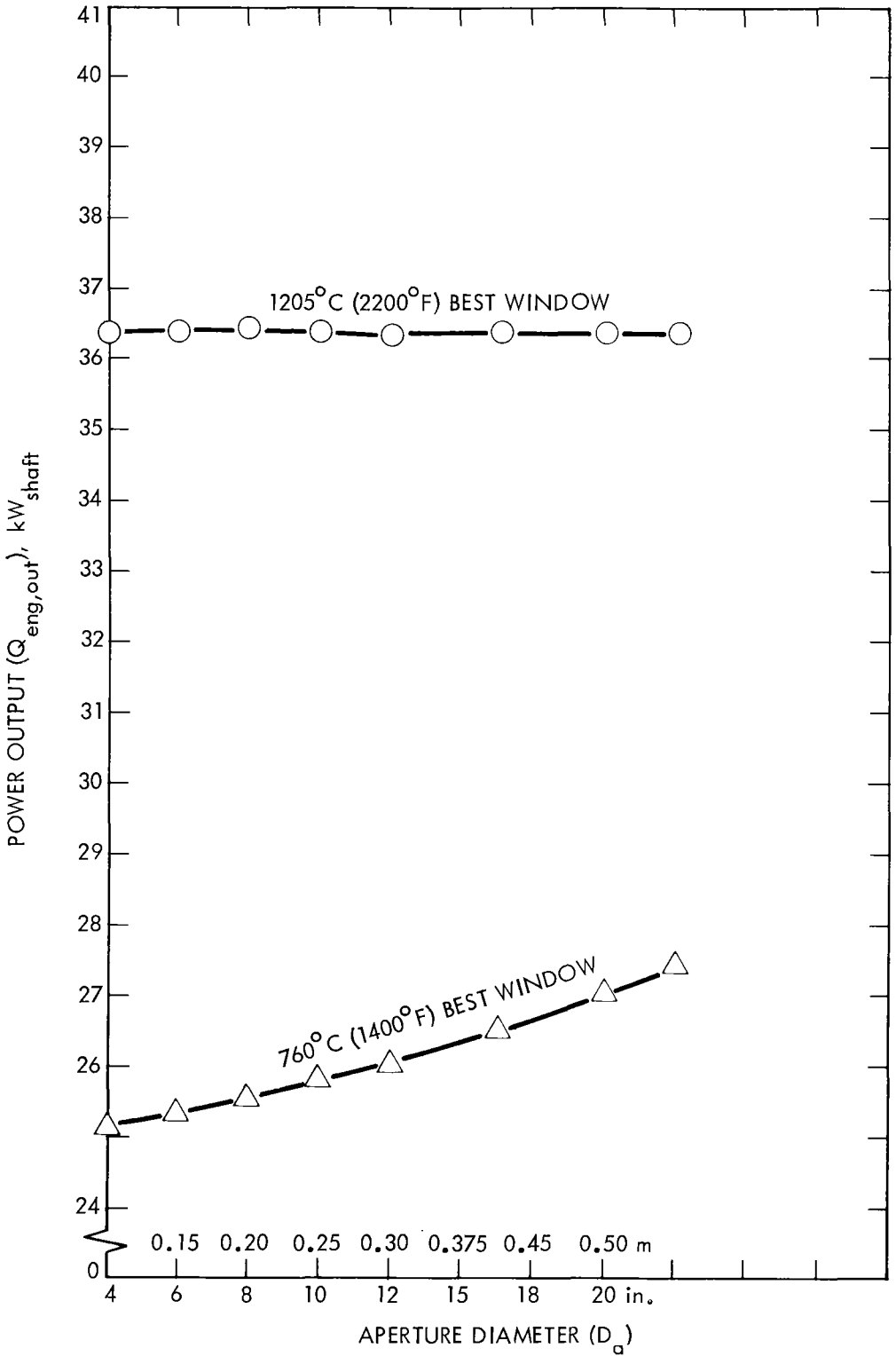

Figure 3-5. Brayton Engine Shaft Power Output versus D_a

d. Stirling Engine Receiver Performance. Figure 3-6 represents the heat input and output values for the open-cavity Stirling receiver; Figure 3-7, the net shaft work produced by the kinematic 4-95 Stirling engine at 980°C (1800°F) and at 760°C (1400°F). It should be noted that the shaft work decreases with increasing aperture size because receiver losses increase correspondingly.

Stirling engine output varies from 40 to 30.3 kW_{shaft} as the aperture size is increased from 0.10 to 0.5 m (4 to 20 in.) for an engine operating at 980°C (1800°F). If the engine temperature is reduced to 760°C (1400°F), which is the value for state-of-the-art engines, the output falls to 34.4 kW_{shaft} for the 0.10-m (4-in.) aperture but rises to 33.2 kW_{shaft} for the 0.5-m (20-in.) aperture.

Figure 3-8 represents heat input and output values for the open-cavity Stirling receiver used in conjunction with the Mod-1 Advanced Automotive Stirling engine, which is the NASA Lewis Research Center's redesign of USAB 4-95 engine, as characterized in Figure 3-2. The heater-head temperature assumed for this engine (720°C or 1328°F) is a little less than that assumed for the USAB 4-95 engine. The net engine output is almost independent of aperture diameter (Figure 3-9). Among the various options studied, this engine option provides the highest efficiency. Power output is also higher for an engine temperature of 760°C (1400°F).

e. Prediction of Engine Outputs. The final step in analyzing the solar power module is to predict the shaft power output of the engine for a given heat input.

According to Figure 3-10, which presents engine efficiency curves as a function of heat output from the receiver to Brayton and Stirling engines, design points for the USAB 4-95 and Brayton engines are taken to be at the 80-kW_t input level. Although Brayton engines could accommodate substantially more input, particularly at 1205°C (2200°F), Stirling engine input could barely exceed the design point by more than 20% at most. This overload is due to the increased working fluid (helium or hydrogen) pressure that is required for constant fluid temperature operation. Increased pressures at these elevated temperatures would tend to result in creep failure of tubes. Damage to bearings and other components are also expected.

In case the nominal thermal input into the engine is increased from 80 kW_t to 90 or 100 kW_t, the shaft output increases proportionally near full load conditions.

A careful examination of Figures 3-6 and 3-7 reveals the fact that variation of engine efficiencies for the Stirling and Brayton engines (operating at 1205°C or 2200°F) in the range of heat input from 80 to 100 kW_t are about +1 to +2.5%. The efficiency of the Brayton engine operating at 760°C (1400°F) varies up to -3.3%; therefore, the variation of the output can be considered linearly proportional to the heat output because the engine efficiency is almost constant near the design point.

At 80-kW input (0.2-m, 8-in. aperture):

(1) Brayton - 1205°C (2200°F): 36.4 kW_{shaft}
760°C (1400°F): 25.5 kW_{shaft}

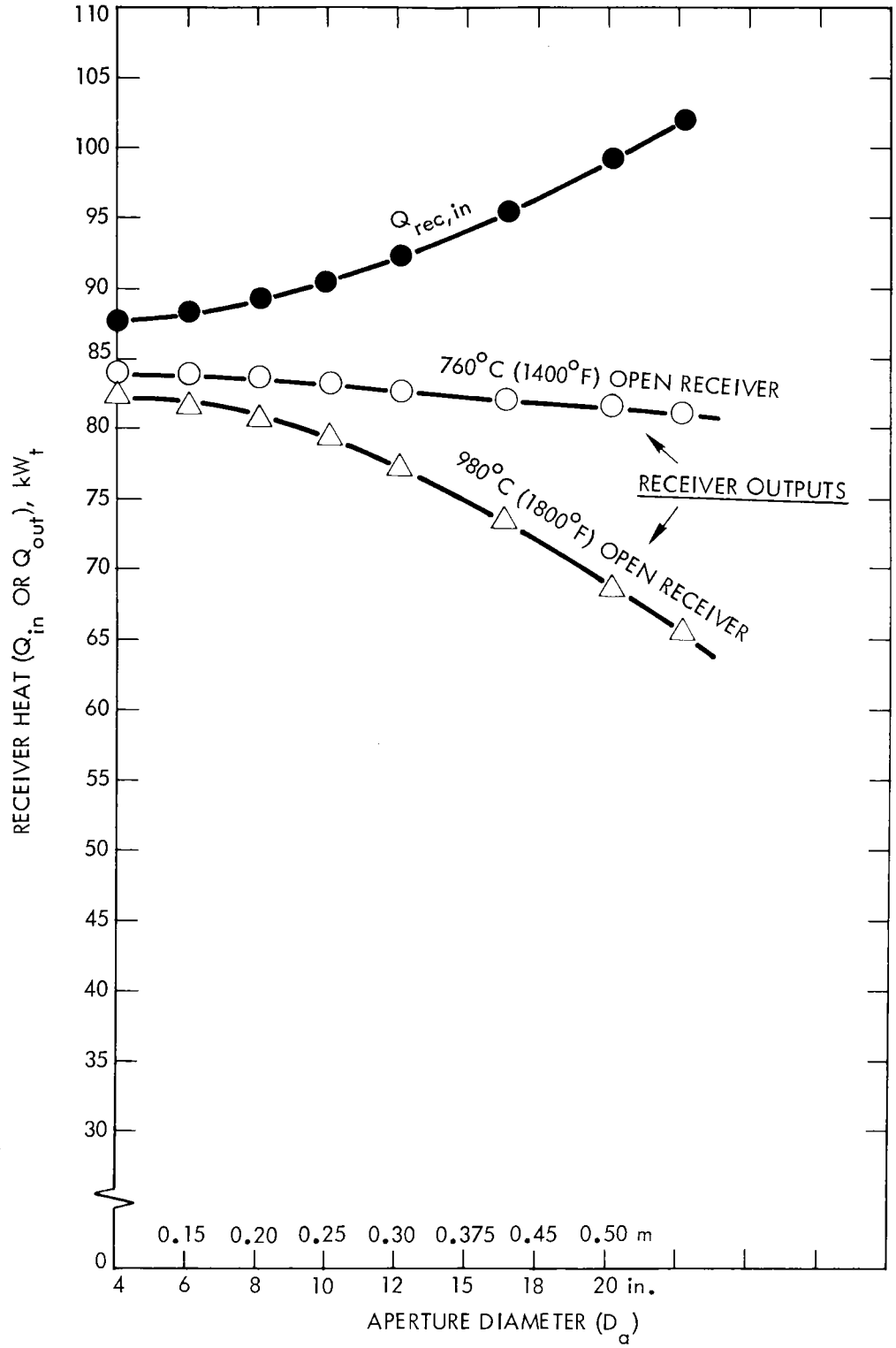

Figure 3-6. Receiver Heat Input/Output for Stirling 4-95 Engine

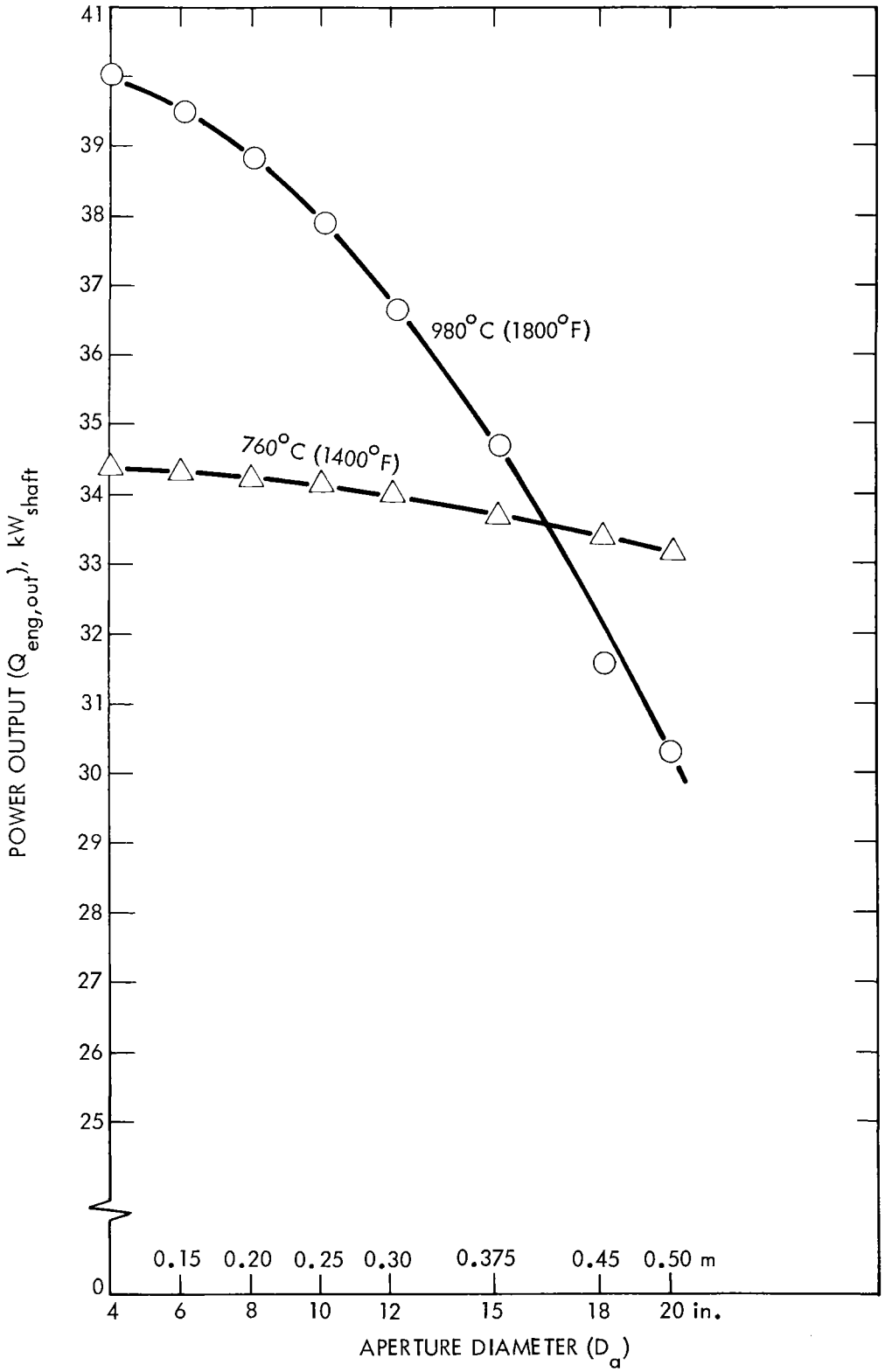

Figure 3-7. Stirling 4-95 Engine Shaft Power Output versus D_a

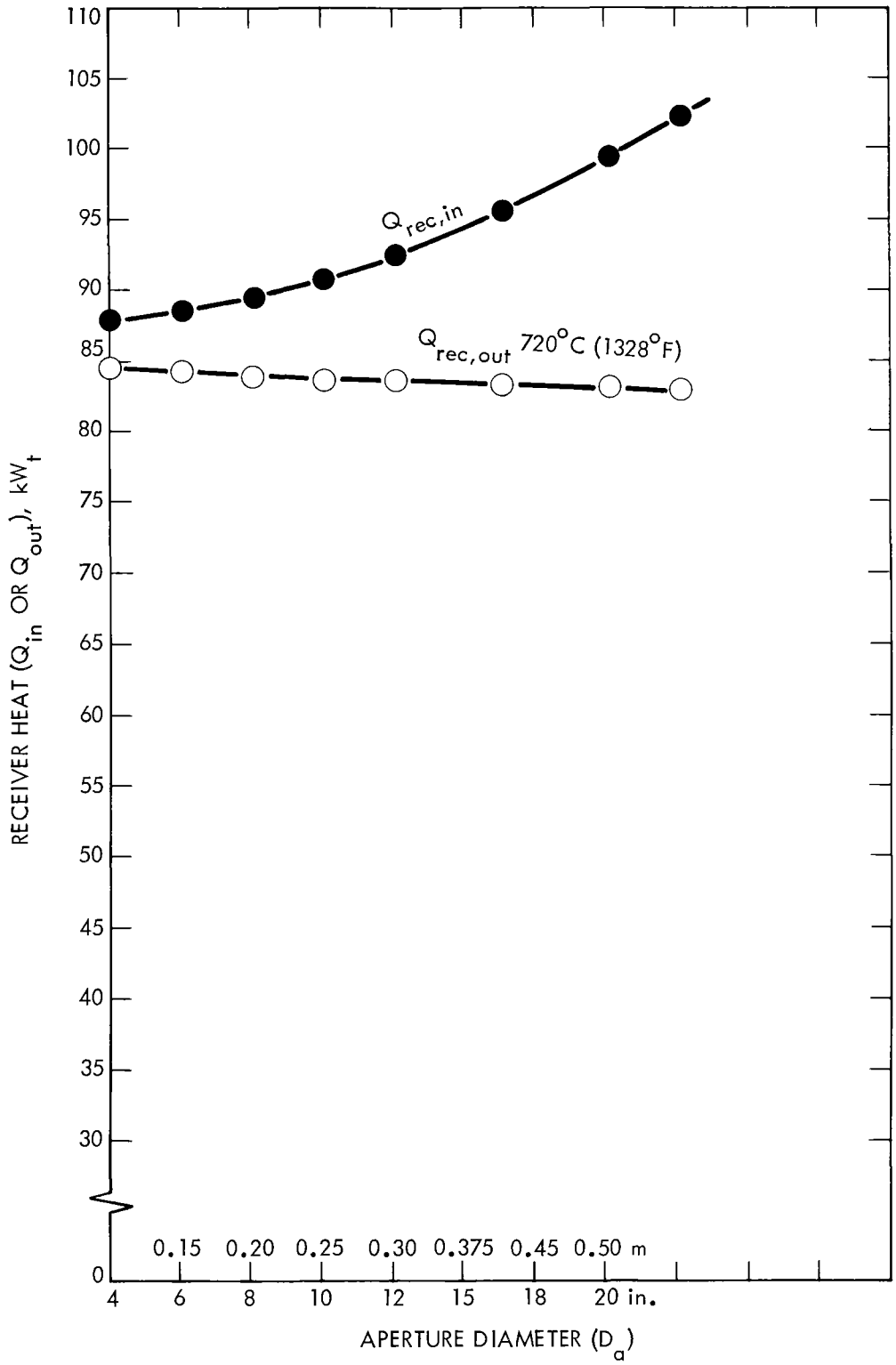

Figure 3-8. Receiver Heat Input/Output for Automotive Stirling Mod-1

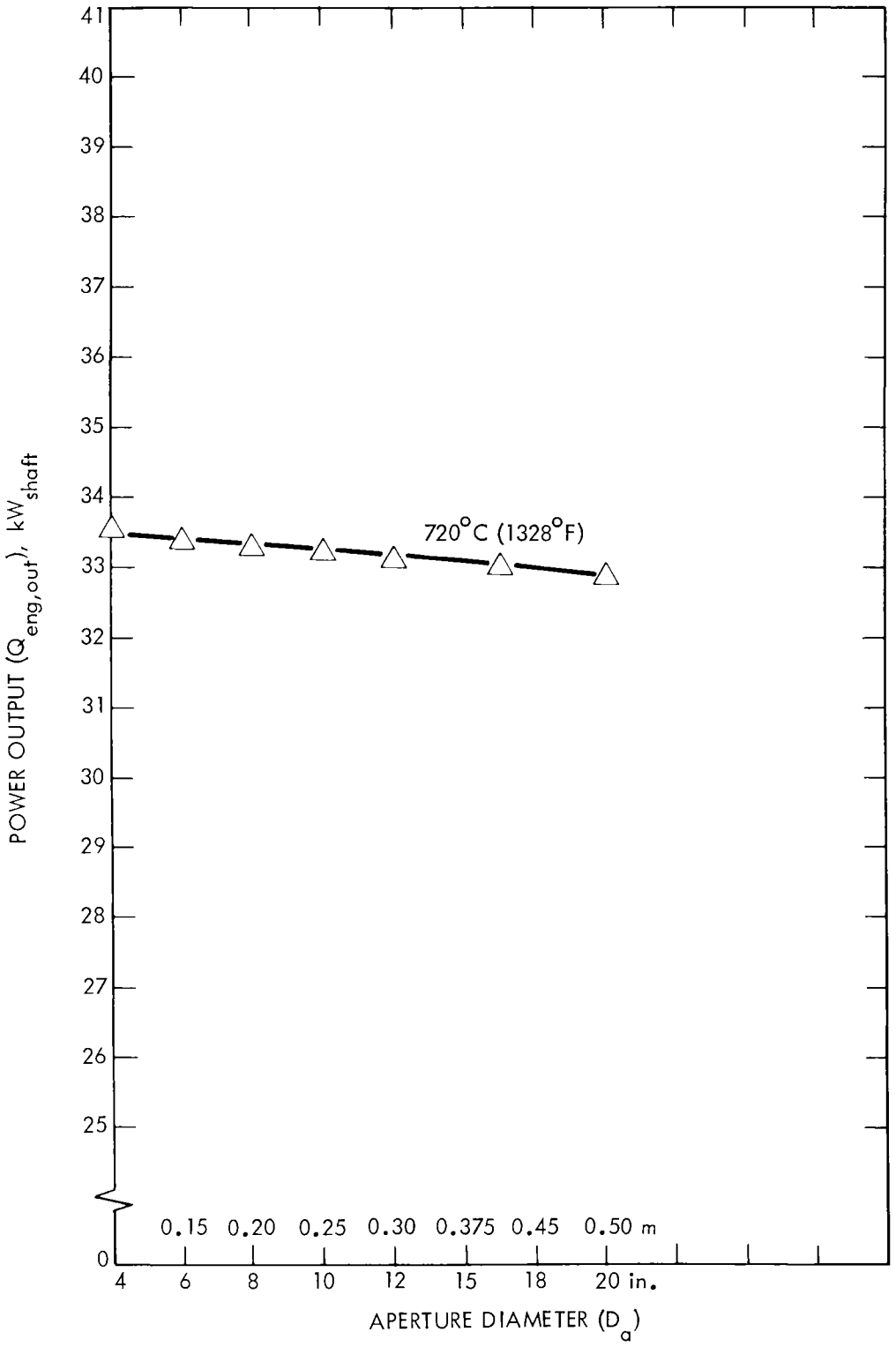

Figure 3-9. Automotive Stirling Mod-1 Engine Shaft Power Output versus D_a

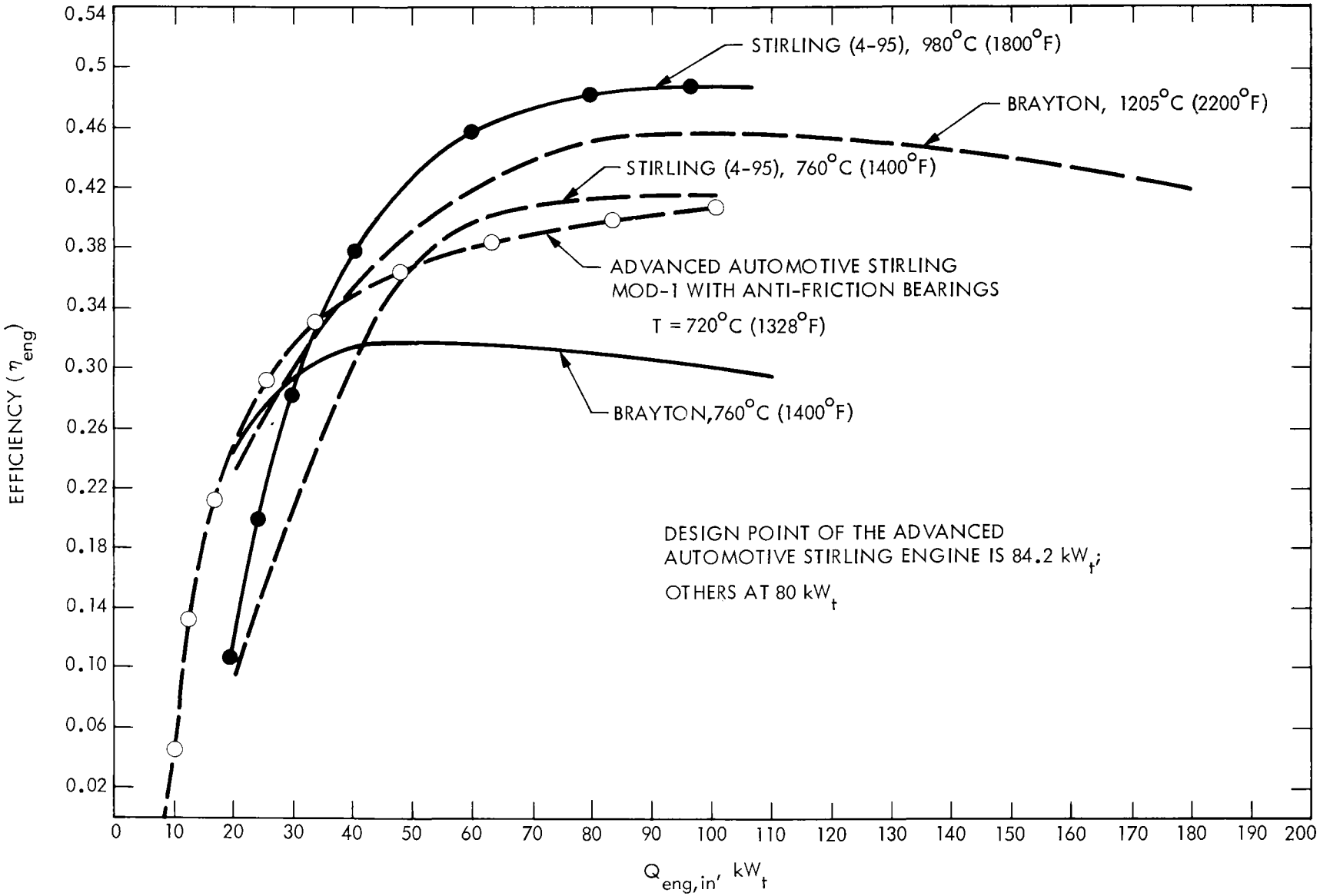

Figure 3-10. Engine Efficiencies versus Heat Input (η_{eng} vs $Q_{in,eng}$)

(2) Stirling - 980°C (1800°F): 38.8 kW_{shaft}
760°C (1400°F): 34.2 kW_{shaft}

(3) Automotive
Stirling - 720°C (1328°F): 33.2 kW_{shaft}

At 90-kW_t input (0.2-m, 8-in. aperture): Simple ratio

(1) Brayton - 1205°C (2200°F): 36.4 x 90/80 = 40.95 kW_{shaft}
760°C (1400°F): 25.5 x 90/80 = 28.6 kW_{shaft}

(2) Stirling - 980°C (1800°F): 38.8 x 90/80 = 43.65 kW_{shaft}
760°C (1400°F): 34.2 x 90/80 = 38.47 kW_{shaft}

(3) Automotive
Stirling - 720°C (1328°F): 33.2 x 90/80 = 37.35 kW_{shaft}

More accurate results of the calculations of the shaft power outputs are presented below for Q_{in} = 90 kW_t.

(1) Brayton - 1205°C (2200°F): 40.9 kW_{shaft}
760°C (1400°F): 28.57 kW_{shaft}

(2) Stirling - 980°C (1800°F): 43.34 kW_{shaft}
760°C (1400°F): 38.34 kW_{shaft}

(3) Automotive
Stirling - 720°C (1328°F): 37.5 kW_{shaft}

Differences between the results obtained by factoring the shaft outputs for 80 kW_t by (90/80) are negligible.

Because the design point efficiency curves for the selected engines are rather flat in the vicinity of 80 kW_t input, small inaccuracies in heat loss predictions and the resulting errors in the heat input values do not significantly alter the engine conversion efficiencies. The present example delineates the guidelines that are used in selecting the size of the concentrator and its characteristics. If concentrator design and operational constraints dictate a design point in the vicinity of the nominal design point, then this can be accommodated easily without compromising conversion efficiency.

SECTION IV

ANALYTICAL FOUNDATION OF THE NOMOGRAM

This section presents the analytical foundation of the nomogram in terms of the mathematical modeling relations used to represent each major component of the parabolic dish systems. The basic assumptions used in deriving the relationships are given so that it will be possible to readily update the nomogram at a future time in order to reflect changes in projected component characteristics or refinements in modeling relations.

The modeling relations used in developing the nomogram are subdivided into three groups comprising the relations that characterize the concentrator, receiver, and engine.

A. CONCENTRATORS

The concentrator performance depends upon two factors: (1) the optical performance of the mirror assembly and (2) the thermal performance of the receiver. In this section these are discussed separately; therefore, the concentrator performance characterized by the optical efficiency (η_o) relation will be discussed first.

The optical efficiency is:

$$\eta_o = \phi G \rho \alpha \tag{8}$$

where ϕ is the intercept factor, G is the geometric shading factor, ρ is the reflectance of the mirror surface, and α is the effective absorptance of the cavity receiver. The intercept factor is defined as the ratio of the energy incident upon a given aperture to the total energy that would have been captured if the aperture were infinitely large. The optical efficiency term is dominated by the intercept factor ϕ. G is related to the shading geometry, ρ is the reflectance of the mirror surface, and α is related to the receiver design and the optical properties of the interior surface. The optical efficiency is the highest possible value of the combined concentrator/receiver efficiency attained if a perfect receiver, i.e., one having no thermal losses, were placed in the focal plane.

Cold water cavity calorimetry is used to determine the optical efficiency of parabolic dish concentrators. The working fluid, water, which is introduced at slightly below or at ambient temperature and circulated at high flow rates, attains only a very small temperature rise and thus the receiver heat losses are almost totally eliminated. Therefore, the enthalpy rise is almost equal to the heat input into the receiver. Instead of independent determination of ρ, ϕ, G, and α, a single test can be run using a cold water cavity calorimeter for finding the optical efficiency. Test results can be used directly for system performance predictions or verification of the optical models. The intercept factor for a manufactured parabolic dish also can be determined by optical methods. Experimental methods of determination of the optical quality of

parabolic dishes and the test results using JPL's 25-ft space simulator are presented in Reference 15.

Optical analysis of parabolic concentrators requires information on the mirror surface slope and pointing errors. Calculation methods for flux intensity distribution and intercept factors have been developed for concentrators with known slope and pointing errors (Refs. 10, 11, 13, and 14). These calculations, however, are tedious. Rather than calculating the intercept factor for each specific design, utilizing curves like those presented in Figure 4-1 (adapted from Ref. 11) would be more convenient, and the accuracy of the calculations would be acceptable. Wen, et al, gives an excellent review of the literature on the optics of parabolic dish-type solar concentrators (Ref. 11). Computer programs have been developed and run several times at JPL for focal plane flux distribution analyses (Refs. 16 and 17).

Figure 4-1, adapted from Reference 11, compares intercept factor values calculated by a numerical method and the Duffie/Aparisi equation. The focal plane flux intensity, J, is divided by the input flux, ρI_b, and plotted against r_x/R, where r_x is the radial distance from the center and R is the radius of the mirror. The effect of the reflecting surface errors on the flux distribution at the focal plane is also seen in Figure 4-1. A numerical method and the contour error method are compared.

The collector portion of the nomogram proposed, gives ρ and ϕ relations in chart form. G, the shading factor, can be calculated from the mirror, receiver, and its supporting structure geometry. α can be obtained from the receiver dimensions and the absorptance of the inside coating.

In an earlier publication by the author (Ref. 12), another nomogram was presented to determine ϕ, ρ, G, and α graphically with reasonable accuracy (Ref. 12). The same nomogram also gives typical beam radiation data for clear-sky conditions at 36-deg N latitude, charts for determining overall collector efficiency, and the amount of useful heat collected. The Appendix gives the nomogram that is discussed.

B. RECEIVER PERFORMANCE

The performance of the receiver alone is expressed mathematically as follows:

$$\eta_{rec} = \frac{Q_{out,rec}}{Q_{in,rec}} = \frac{Q_{in,rec} - Q_{loss}}{I_c A_c \rho G \phi \alpha} \tag{9}$$

where η_{rec} is the receiver efficiency, $Q_{in,rec}$ and $Q_{out,rec}$ are heat input to and output from the receiver, respectively. The receiver loss, Q_{loss}, per unit aperture consists of the following contributions:

(1) Radiation: $(\varepsilon h_r)\ \Delta T$

(2) Convection: $(h_c)\ \Delta T$

(3) Conduction: $(h_k)\ \frac{A_{rw}}{A_a}\ \Delta T$

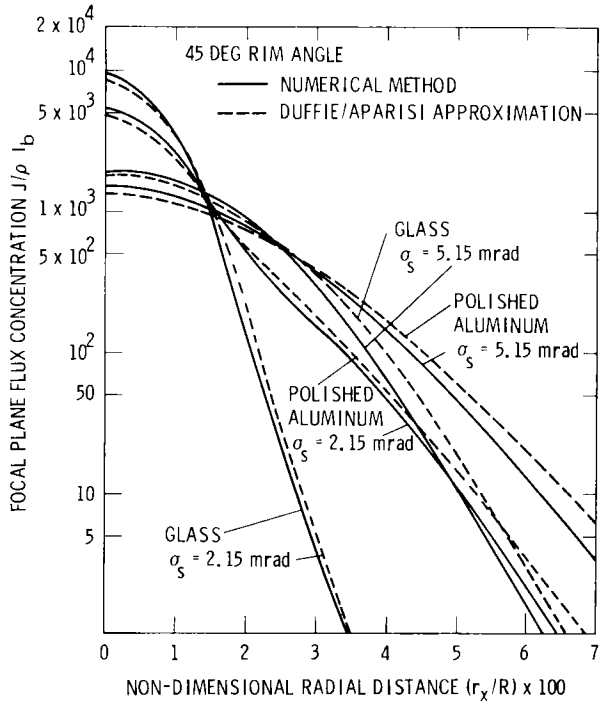

(a) Comparisons of Focal Plane Flux Distributions with Duffie/Aparisi Equation

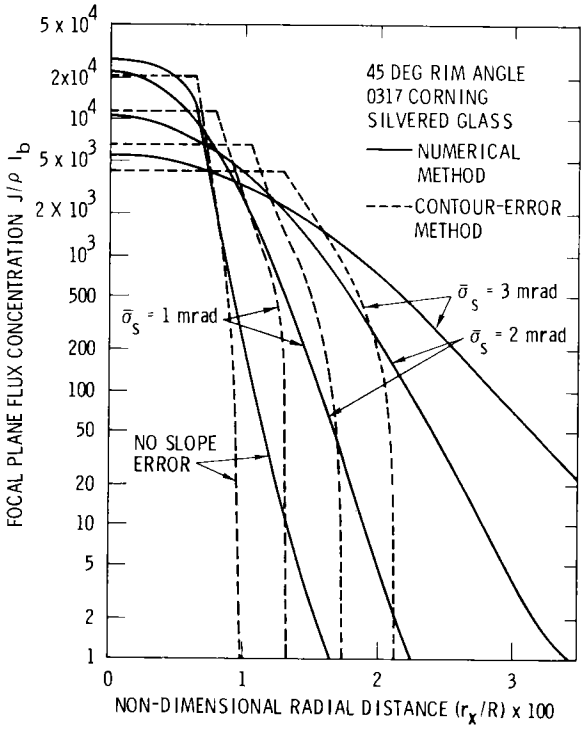

(b) Comparison of Focal Plane Flux Distributions with Contour Error Method

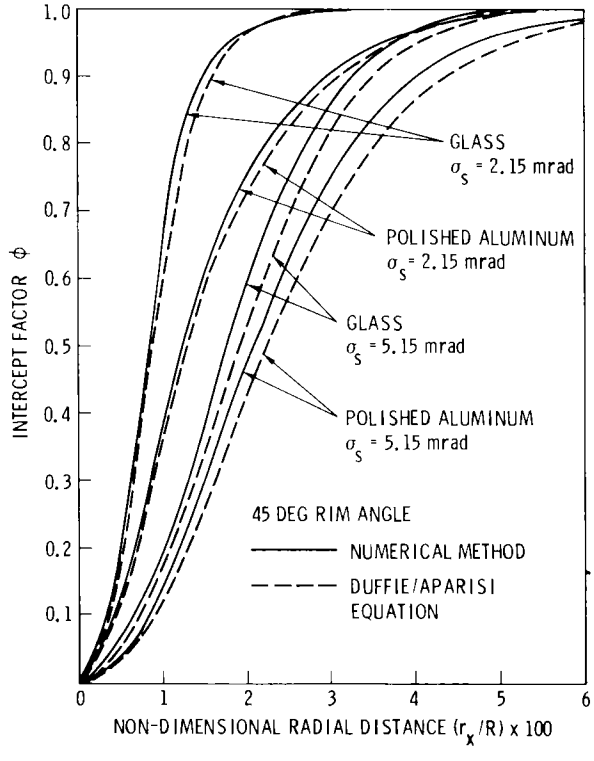

(c) Duffie/Aparisi Approximations of Intercept Factor

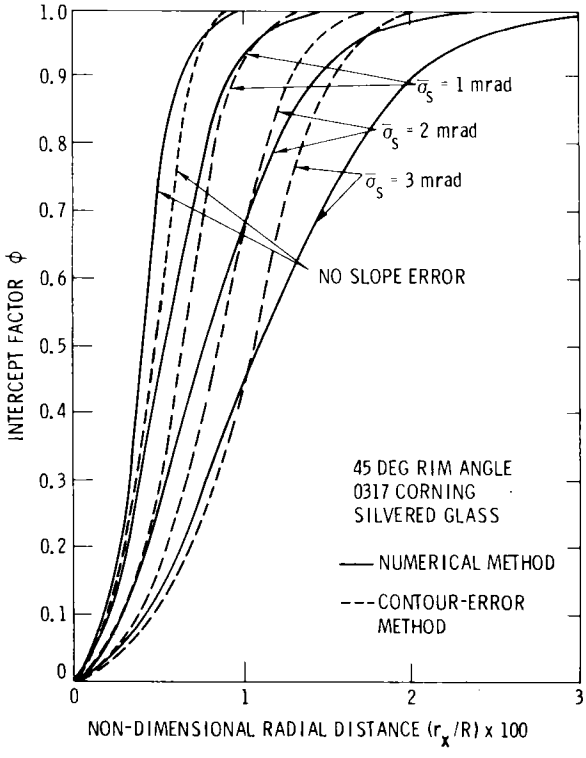

(d) Intercept Factor Approximations by Contour Error Method

Figure 4-1. Intercept Factor Curves

where ε is the effective emittance of the cavity receiver, h_r is the equivalent radiative heat transfer coefficient, h_c is the convective heat loss coefficient expressed in terms of aperture area, h_k is the conductance of the insulated receiver wall, and A_{rw} and A_a are the wall and aperture areas, respectively.

Both open and windowed receivers have been examined. Highlights of the mathematical models of energy balances of open and windowed receivers are presented below.

1. Performance of Open Receivers

Heat loss from the open cavity calculated for several receiver temperatures, as a function of the aperture diameter, are presented in Figure 4-2. Losses consist of convection, conduction, and reradiation losses. Convection losses are dependent upon the receiver geometry, orientation, aperture size, and wind speed and direction. In this study, receiver convection losses were predicted on the basis of empirical relations developed by Dr. A. Clausing of the University of Illinois (Ref. 18). The convection losses were calculated for zero wind conditions because no quantitative data or empirical relations to determine the contribution of the wind blowing from any direction were available. Test runs, with a mock-up receiver installed at the focal point and oriented to different directions with respect to the wind vector, are needed for accurate determination of the convection losses.

In Figure 4-2, approximately 1% of the incoming energy flux is assumed to be lost as direct reflection for a 0.38-m (15-in.) aperture. Thus, the reflection losses were considered to be directly proportional to the aperture area. Total losses ranged from 2.4 kW_t for a 0.1-m (4-in.) aperture to 14.9 kW_t for a 0.5-m (20-in.) aperture for the open receiver at an operating temperature of 645°C (1200°F). These losses increase to 3.8 and 36.44 kW_t, respectively, when the receiver cavity temperature is raised to 980°C (1800°F).

2. Performance of the Receiver with a Window

Addition of a transparent window to an open receiver eliminates the influx of cold ambient air into the cavity. This flux would leave the cavity after being heated and, thus, result in heat loss from the receiver. Wind, particularly gusty wind, increases this mode of heat loss. Heat losses from the receiver cavity with a quartz-windowed aperture were calculated for window absorptance values of 0.01 and 0.02 and window reflectance values of 0.04, 0.06, and 0.08. The corresponding apparent transmittance values varied from 0.90 to 0.95. Quartz was selected as the preferred window material because of its high transmittance, its low thermal conductivity and thermal expansion coefficient, and its resistance to thermal shock at high temperatures. Variation of optical properties with wavelength was taken into consideration by using different transmittance and absorptance values below and above cutoff wavelength. This wavelength was assumed to be $\lambda = 4\mu$.

The energy balance of the quartz window was determined by calculating the heat gain by absorption of shortwave incoming and longwave outgoing radiation, and by convection from the inside of the cavity. The window looses heat to its surroundings by convection and reradiation. Some fraction of the longwave

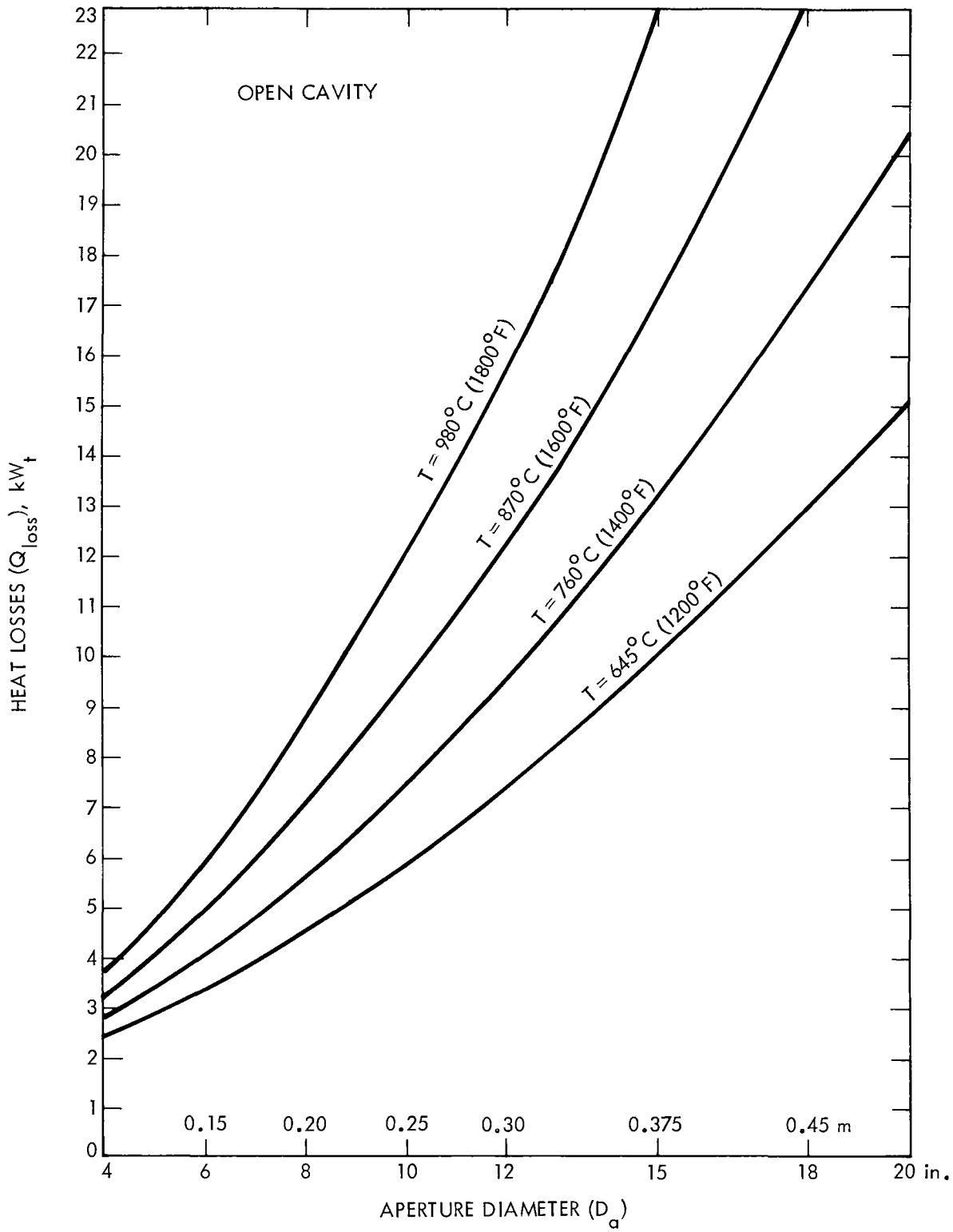

Figure 4-2. Heat Losses from an Open Receiver versus Aperture Diameter

outgoing radiation, i.e., radiation at $\lambda < 4.0\mu$, is directly transmitted through the window. Some small fraction (less than 1%) of the incoming short-wave radiation is lost by cavity reflection.

The receiver window analysis was carried out using a one-dimensional heat transfer model. Although the flux pattern of the concentrated solar radiation is not uniform and this nonuniformity will cause some radial temperature variations, a simplified one-dimensional model is believed to be sufficient.

The temperature of the quartz window was assumed to be uniform. Due to the complexity of the two-dimensional heat transfer model of the quartz window and because the ultimate objective of the study is to determine window losses approximately, the actual window temperature distributions were not investigated. Such modeling enables results to be obtained much faster and within 10% accuracy, which has been specified as acceptable.

Energy balance equations for the window were written and solved for the following three combinations of absorptance and reflectance values for the quartz window. The transmittance, τ, for $\lambda > 4\mu$ was assumed to be negligible. Other optical properties for $\lambda < 4\mu$ are listed below:

(1) Best window:

(a) Absorptance, $\alpha_w = 0.01$

(b) Reflectance, $\rho_w = 0.04$

(c) Transmittance, $\tau = 0.95$

(2) Intermediate window:

(a) Absorptance, $\alpha_w = 0.01$

(b) Reflectance, $\rho_w = 0.06$

(c) Transmittance, $\tau = 0.93$

(3) Worst window:

(a) Absorptance, $\alpha_w = 0.02$

(b) Reflectance, $\rho_w = 0.08$

(c) Transmittance, $\tau = 0.90$

These values assume a clean window. Ultimately, the effects of dirt accumulation and coating of the inside of the window with volatile material discharged from the cavity surfaces should be considered; however, these effects have not been evaluated here because a more simplified approach is utilized. Figure 4-3 shows heat losses as a function of the aperture diameter for three types of windows.

Findings are summarized below for minimum and maximum temperatures and aperture sizes:

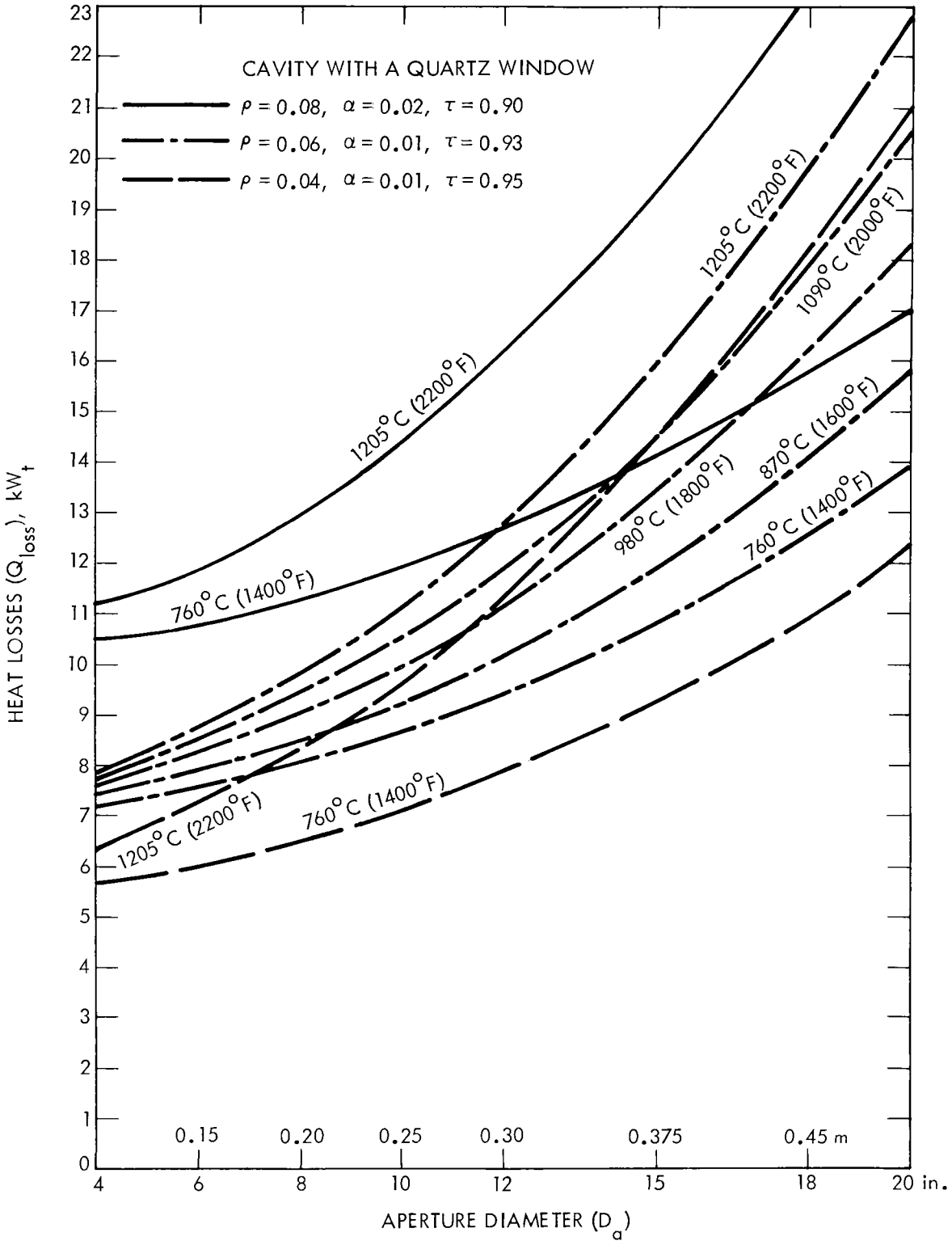

Figure 4-3. Heat Losses from a Cavity with Window versus Aperture Diameter

(1) Best window:

(a) At T = 760°C (1400°F), Q_{loss} = 5.7 kW_t for 0.10 m (4 in.) and Q_{loss} = 12.5 kW_t for 0.5 m (20 in.)

(b) At T = 1205°C (2200°F), Q_{loss} = 6.4 kW_t for 0.10 m (4 in.) and Q_{loss} = 21.4 kW_t for 0.5 m (20 in.)

(2) Intermediate window:

(a) At T = 760°C (1400°F), Q_{loss} = 7.2 kW_t for 0.10 m (4 in.) and Q_{loss} = 14.1 kW_t for 0.5 m (20 in.)

(b) At T = 1205°C (2200°F), Q_{loss} = 8.0 kW_t for 0.10 m (4 in.) and Q_{loss} = 22.9 kW_t for 0.5 m (20 in.)

(3) Worst window:

(a) At T = 760°C (1400°F), Q_{loss} = 8.8 kW_t for 0.10 m (4 in.) and Q_{loss} = 15.6 kW_t for 0.5 m (20 in.)

(b) At T = 1205°C (2200°F), Q_{loss} = 9.6 kW_t for 0.10 m (4 in.) and Q_{loss} = 24.5 kW_t for 0.5 m (20 in.)

The quartz window improves performance if the absorptance value is low for a given thickness. Higher absorptance increases the window equilibrium temperature, which increases receiver losses.

Figure 4-4 is a plot of the window temperature as a function of the aperture diameter for selected values of ρ, α, and τ.

C. CONCENTRATOR/RECEIVER COMBINATION

For the concentrator/receiver combination, the collector efficiency and useful heat relations are:

$$\eta_c = \phi\rho G\alpha - \frac{(\varepsilon h_r + h_c + A_{rw}/A_a\, h_k)\ \Delta T}{I_b \cdot CR} = a - b\,\frac{\Delta T}{I_b} \qquad (10)$$

$$\eta_c = \eta_o - Q_{L,rec}/(I_b \cdot CR) \qquad (11)$$

$$Q_u = I_b \cdot A_c \cdot \eta_c \qquad (12)$$

In these equations, I_b is the intensity of the beam radiation, CR is the concentration ratio, and ΔT is $(T_{collector} - T_{ambient})$. The optical efficiency, η_o, is represented by "a," and the overall heat loss coefficient is represented by "b." Q_u is the useful heat per unit area.

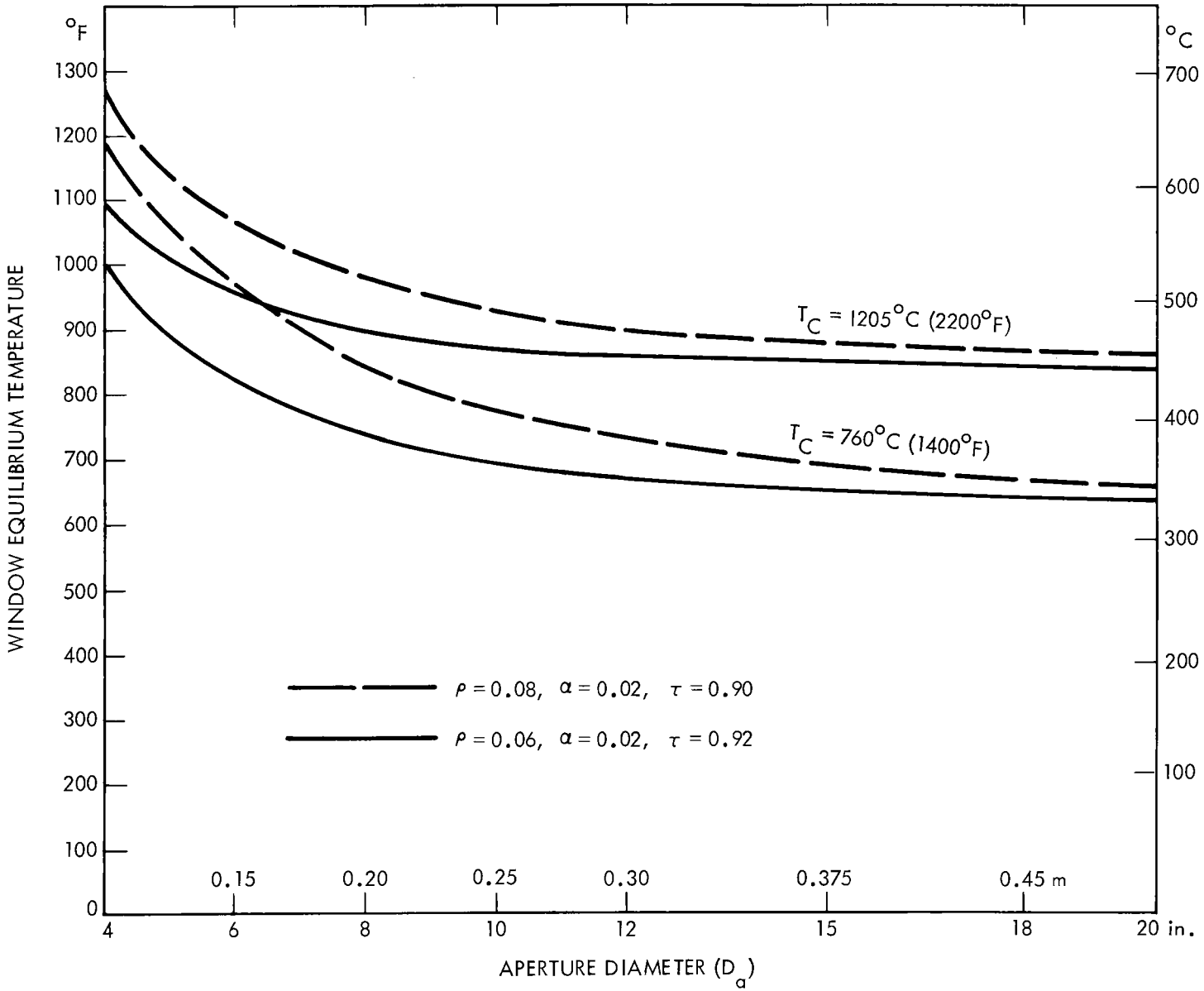

Figure 4-4. Receiver Window Temperature

In Equation (10), the first term "a," the optical efficiency, characterizes the concentrator, whereas "b" is dependent upon the design and operating conditions of the receiver.

D. THE PERFORMANCE OF BRAYTON AND STIRLING ENGINES

Engine performance analysis presented in this report requires a knowledge of the thermal conversion efficiency, i.e., the ratio of the shaft work to the heat input to the engine only. Therefore, selection of other design and operational factors such as speed, dimensions, working fluid, etc., were not attempted.

Brayton and Stirling engine performance results have been selected from previous studies undertaken as a part of the Brayton and Stirling module development programs managed by JPL.

Because the engines are expected to operate from full load to idling conditions, engine performance is examined under the name of "part-load performance" (next section).

E. ENGINE PART-LOAD PERFORMANCE

Engine efficiency is defined as

$$\eta_{eng} = \frac{W_{out,eng}}{Q_{in,eng}} = \frac{Q_{in,eng} - Q_{loss,eng} - W_{friction}}{Q_{in,eng}} \qquad (13)$$

where $W_{out,eng}$ is the net shaft output power of the engine.

Part-load characteristics of each engine are presented in the following paragraphs and figures.

The Brayton engine part-load characteristics were given in Figure 3-1 for turbine inlet temperatures of 1205°C (2200°F) and 760°C (1400°F). Nominal efficiency values at the design points are $\eta_o = 0.45$ and $\eta_o = 0.31$, respectively.

The Stirling engine part-load characteristics were given in Figure 3-2 for a heater-head temperature of 720°C (1328°F) for the USAB 4-95 Stirling engine and the automotive AGT Mod-1 Stirling engine with anti-friction bearings.

Heat input versus engine efficiency curves for the baseline Brayton and Stirling engines were presented previously in Figure 3-10. Operating temperatures, i.e., turbine inlet temperatures, for the Brayton engine have been designated as 760°C (1400°F) and 1205°C (2200°F). Stirling engine characteristics have been projected at 760°C (1400°F) and 980°C (1800°F) for the 4-95 model and at 720°C (1328°F) for the advanced automotive Mod-1 with anti-friction bearings.

At the selected design points, the nominal heat input to these engines is 80 kW_t, except for the Mod-1 engine, which has a design value of 84.2 kW_t. It should be noted that Brayton engines have rather flat efficiency curves ranging

from 40 to 100 kW_t at 760°C (1400°F), and 60 to 180 kW_t at 1205°C (2200°F). This feature provides an advantageous flexibility in design considerations.

F. OVERALL SYSTEM PERFORMANCE

Overall system efficiency is given by

$$\eta_{sys} = (W_{out,eng}/I_b \cdot A_c) \tag{14}$$

The product of I_b and A_c is the incident insolation on the projected net area of the parabolic dish concentrator.

The net shaft output may be determined from Figure 3-10 by entering with the $Q_{in,eng}$ value and intersecting with the curve corresponding to the type of engine and its operating temperature. This gives the engine efficiency, η_{eng}, which is then multiplied by $Q_{in,eng}$ to obtain shaft work output. If the engine is coupled to an alternator, additional power losses have to be considered by multiplying the shaft work output by η_{alt} to determine the module electrical output. Usually, additional losses occur due to power conditioning equipment. For example, sometimes it is necessary to convert high frequency ac to dc, then back to 60-Hz ac.

SECTION V

DISCUSSION AND CONCLUSIONS

Because the nomogram presented is graphical in nature, it enables an investigator to quantify quickly the sensitivity of the system performance to the design and operational parameters.

The performance of the components of the module are clearly interrelated. The selection of several design and operation parameters influences the performance of all subsystems. Further discussion on the most important parameters is given below.

A. CONCENTRATOR PARAMETERS

Concentrator size determines the maximum collectible heat, which determines the shaft work produced by the engine. Both the concentrator/receiver and engine outputs are directly proportional to the concentrator size. The net output of each component is reduced by an amount determined by the shading factor, G. Similarly, the reflectance, ρ, accounts for the decrease in the intensity of the flux reflected from the concentrator as compared to the solar flux impinging on the concentrator.

The most important factor in determining the net concentrator output is the intercept factor, ϕ. The receiver input is also determined by ϕ. The intercept factor is dependent mainly upon the mirror surface accuracy, concentrator tracking and receiver positioning errors, specularity of the reflector surface, and the receiver aperture size.

An improperly selected intercept factor will cause excessive spillage of the concentrated flux or increased receiver losses. The intercept factor will increase as receiver aperture diameter increases. Thus, a compromise solution must be sought by several iterations to optimize the ϕ value.

B. RECEIVER PARAMETERS

Once a receiver aperture size is selected, losses could be reduced significantly by improving the insulation. Some reduction of convection may be possible either by adding outer windshields or by modifying the receiver inner configuration and surface coatings. Improved insulation reduces the conduction losses. Particularly with open cavity receivers, convection and reradiation may be reduced through advanced design for a fixed aperture. Receivers with windows eliminate convection losses but introduce transmission losses. Reradiation losses are reduced but still contribute significantly to the total losses. Receiver losses are sensitive to the variation of transmittance of the window material. BLOCK 9 of the nomogram (Figure 2-2) gives two curves for windowed receivers operating at 760 and 1205°C (1400 and 2200°F), respectively. Additional curves are presented in Figure 2-3, but omitted from Figure 2-2 in order to simplify the nomogram. Heat loss values for other types of receivers and operating temperatures must be obtained from Figure 2-3 and entered into BLOCK 8 at $Q_{loss,rec}$.

C. ENGINE PERFORMANCE PARAMETERS

Part-load characteristics of both Stirling and Brayton engines have been presented (Figure 3-10). Particularly, Brayton engines have rather flat efficiency characteristics, which make them relatively insensitive to heat input. Considering the two types of Stirling engines, advanced designs with antifriction bearings yield the higher efficiencies. Curves are presented at 760 and 980°C (1400 and 1800°F) for the Model 4-95 Stirling engine and 760 and 1205°C (1400 and 2200°F) for the Brayton engine, respectively.

Due to the flat efficiency characteristics, both engines could be used for a wide range of heat inputs, which suggests that a variety of concentrator sizes could match the engine requirements. Other types of engines may be considered. The general nomogram could still be used if the relation between the heat input and the engine output is known or specified. Graphical representation of this new engine relation could be inserted into the nomogram. If the concentrator design and reflector material properties substantially differ from the curves presented herein, then the nomogram can be modified to adopt this more relevant information.

SECTION VI

REFERENCES

1. Wu, Y.C., and Wen, L.C., "Solar Receiver Performance of a Point-Focusing Collector System," ASME Winter Annual Meeting, San Francisco, CA, Dec. 1978, Paper No. 78-WA/SOL-5.

2. Lansing, F.S., HEAP Heat Energy Analysis Program, A Computer Model Simulating Solar Receivers, JPL Publication #79-3, Jan. 15, 1979.

3. Maynard, D.P., and Gajanana, B.C., Analytical Foundations/Computer Model for Dish Brayton Power Systems, JPL Report No. 5105-9, Sept. 1980.

4. Jaffe, L.D., Optimization of Dish Solar Collectors With and Without Secondary Concentrators, JPL Publication #82-103, May 15, 1982.

5. Greaven, M., and Owen, W., "The Development of an 85-kW (Thermal) Air Brayton Solar Receiver," Second Parabolic Dish Solar Thermal Power Annual Program Review Proceedings, Pasadena, CA, Jan 13-15, 1981, pp. 57-65, DOE/JPL-1060-46.

6. Hanseth, E.J., "Development, Solar Test, and Evaluation of a High-Temperature Air Receiver for Point-Focusing Parabolic Dish Applications," Proceedings AIAA Meeting, Dec. 1-3, 1981, Colorado Springs, CO.

7. Wright, C.C., and Bank, H., "The Development of 85-kW (Thermal) Steam Rankine Solar Receiver," Second Parabolic Dish Solar Thermal Power Annual Program Review Proceedings, Pasadena, CA, Jan 13-15, 1981, pp. 67-74, DOE/JPL-1060-46.

8. Osborn, D.B., et al, "Design and Test of a Solar Receiver for an Organic Rankine Cycle Engine," ASME Solar Energy Conference Proceedings, Solar Engineering, 1982, pp. 449-457.

9. Starkey, D.J., and Owen, W. L., "The JPL Flux Mapper and the Characterization of Point Focusing Test Bed Concentrators at JPL," ISES Proceedings, Philadelphia, PA, May 1981.

10. Wen, L., "Effect of Optical Surface Properties on High Temperature Solar Thermal Energy Conversion," Journal of Energy, Vol. 3, No. 2, pp. 82-89, March-April 1979.

11. Wen, L., "Comparative Study of Solar Optics for Paraboloidal Concentrators," ASME Journal of Solar Energy Engineering, Vol. 102, pp. 305-315, Nov. 1980.

12. Selçuk, M.K., "A Nomogram for Determining Efficiency and Useful Heat of a Parabolic Dish," Proceedings ISES 1981 Conference, Solar World Forum, pp. 1727-1731, Pergamon Press.

13. Hughes, R.O., "Efficiency Degradation Due to Tracking Errors for Point Focusing Solar Collectors," ASME Paper No. 78-WA/SOL-4, Dec. 1978.

14. Poon, P., and Higgins, S., "Optical Performance of Several Point Focusing Solar Concentrators," American Institute of Chemical Engineers, 86th National Meeting, Houston, TX, April 1979.

15. Dennison, E.W., and Argoud, M.J., "Solar Concentrator Testing in the JPL 25-foot Space Simulator," AIAA Paper No. 81-2534, Dec. 1-3, 1981, Colorado Springs, CO.

16. Poon, P.T., and Higgins, S., "Thermal and Optical Considerations of the Dish-Stirling Electric Generation System," Third International Conference on Alternate Energy Sources, Miami Beach, Florida, December 1980.

17. Wen, L., and Roschke, E.J., "Thermal Response of Solar Receiver Aperture Plates During Sun Walk-Off," AIAA/ASME Fluids, Plasma and Thermophysical Heat Transfer Conference, St. Louis, MO, June 1982.

18. Clausing, A.M., "Convective Losses from Cavity Solar Receivers, Comparison Between Analytical Predictions and Experimental Results," ASME Solar Engineering, 1982, pp. 388-393.

APPENDIX

A NOMOGRAM FOR DETERMINING EFFICIENCY AND USEFUL HEAT OF A PARABOLIC DISH[1]

A graphical method is presented for calculating the collection efficiency, η_c, and useful heat, Q_u, of a parabolic dish-type solar concentrator based on

$$\eta_c = \phi G \rho \alpha - [\varepsilon h_r + h_c + (A_{rw}/A_a)\, h_k]/I_b CR \quad \text{and} \quad Q_u = \eta_c \cdot I_b \qquad (A\text{-}1)$$

A. INTRODUCTION

A simple calculation tool for easy, but considerably accurate determination of the thermal efficiency of parabolic dish concentrators is offered. Some of the reasons to use a nomogram instead of a computer are

(1) Computer codes for the detailed optical and thermal modelling of parabolic dishes are complicated and expensive to run simply to determine the sensitivity of design and operational parameters.

(2) Many engineers are often asked to give quick answers with reasonable accuracy.

(3) New engineers can learn faster using a general purpose calculational tool that gives a broad view of all factors than by using elaborate computer codes. This matter is quite significant for scientists, engineers, and educators in developing countries. The nomogram allows one to visualize the effects of all design operation factors because it is not a "black-box" approach as are computer codes.

B. DESCRIPTION OF THE NOMOGRAM

The nomogram consists of a main chart and two other components, A and B. The user enters each component of the nomogram at the points indicated in the figures and obtains results simply by following the lines drawn in the directions shown.

The main nomogram, shown in Figure A-1, solves the equation for concentrator efficiency

$$\eta_c = a - b\, \Delta T/I_b \qquad (A\text{-}2)$$

I_b = 800 W/m^2 for October 21 at 16:00 hours, $\Delta T/I_b$ = 0.725, The Slope.

---

[1] Reprinted from Proceedings of the Solar World Forum, International Solar Energy Society Congress and Exhibition, August 23-28, 1981, Brighton, England.

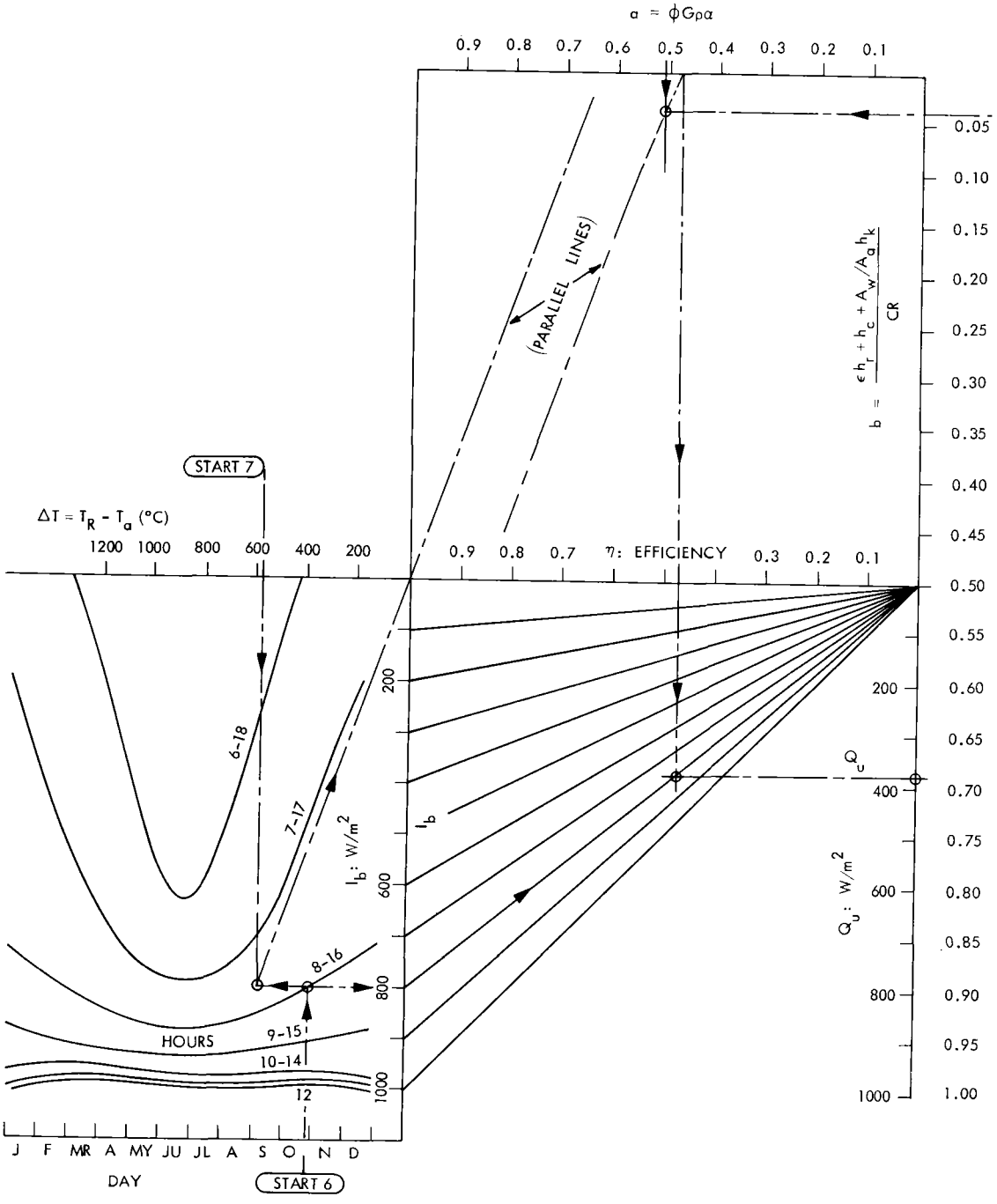

NOTE: The subscript "w" in Figures A-1 through A-3 corresponds to the subscript "rw" of the text.

Figure A-1. Main Nomogram that Determines η_c and Q_u. (It also gives approximate clear-day beam insolation intensity, I_b, at 35 deg latitude.)

The main nomogram is entered with a = 0.51, b = 0.039, and $\Delta T/I_b$ = 0.725.

η_c is obtained by drawing a parallel line from the intersection of (a) and (b) with the line having a slope of $\Delta T/I_b$: η_c = 0.47.

Q_u is obtained from the lower portion of the main nomogram, using 800 W/m^2 line and η_c value: Q_u = 380 W/m^2.

Calculated values are

$\eta_c = a - b\ \Delta T/I_b = 0.51 - 0.039\ (0.725) = 0.472$, Efficiency.

$Q_u = I_b\ \eta_c = 800 \times 0.475 = 377$ W/m^2, Useful Heat.

where $a = \phi G \rho \alpha$, net absorptance (optical efficiency)
ϕ = intercept factor for the receiver
G = receiver shading factor
ρ = reflectance of the mirror surfaces
α = effective absorptance of the receiver aperture.

Figure A-2 is the component A of the nomogram that is used to determine a. The heat loss coefficient, b, is obtained from

$$b = [\varepsilon h_r + h_c + (A_{rw}/A_a)\ h_k\ ]/CR,\ W/m^2\ ^oC$$

where ε = effective emittance of the receiver aperture
h_r = equivalent radiative heat transfer coefficient $= \rho(T_r^4 - T_a^4)/(T_r - T_a)$, W/m^2 ^{o}C
h_c = equivalent convective heat transfer coefficient, W/m^2 ^{o}C
h_k = equivalent conduction heat loss coefficient, W/m^2 ^{o}C
A_a = receiver aperture area, m^2
A_m = mirror area, m^2
CR = concentration ratio = A_m/A_a.

Figure A-3 is the component B of the nomogram that is used to determine b.

$\Delta T = T_r - T_a$, receiver minus ambient temperature, ^{o}C
I_b = beam insolation intensity in W/m^2; could be approximately obtained from Figure A-1, which also gives Q_u, the useful heat, from $Q_u = \eta_c I_b$.

C. EXAMPLE: POLISHED ALUMINUM MIRROR

Enter component A with the following inputs:

D_m = 12 m; receiver envelope diameter, D_{rec} = 1 m; aperture diameter, D_a = 25 cm; focal length, f = 7 m; surface errors, σ_s = 2.15 mrad = 1/8 deg; D_{wall} = 0.4 m; $\alpha = \varepsilon = 0.9$.

Component A yields the optical efficiency, a, together with intermediate results:

Concentration ratio, CR = 2300; intercept factor, ϕ = 0.77; receiver shading factor, G = 0.99; reflectance, ρ = 0.68; A_{rw}/A_a = 9.5; α = 0.98; resulting $\eta_{optical}$ = a = 0.51.

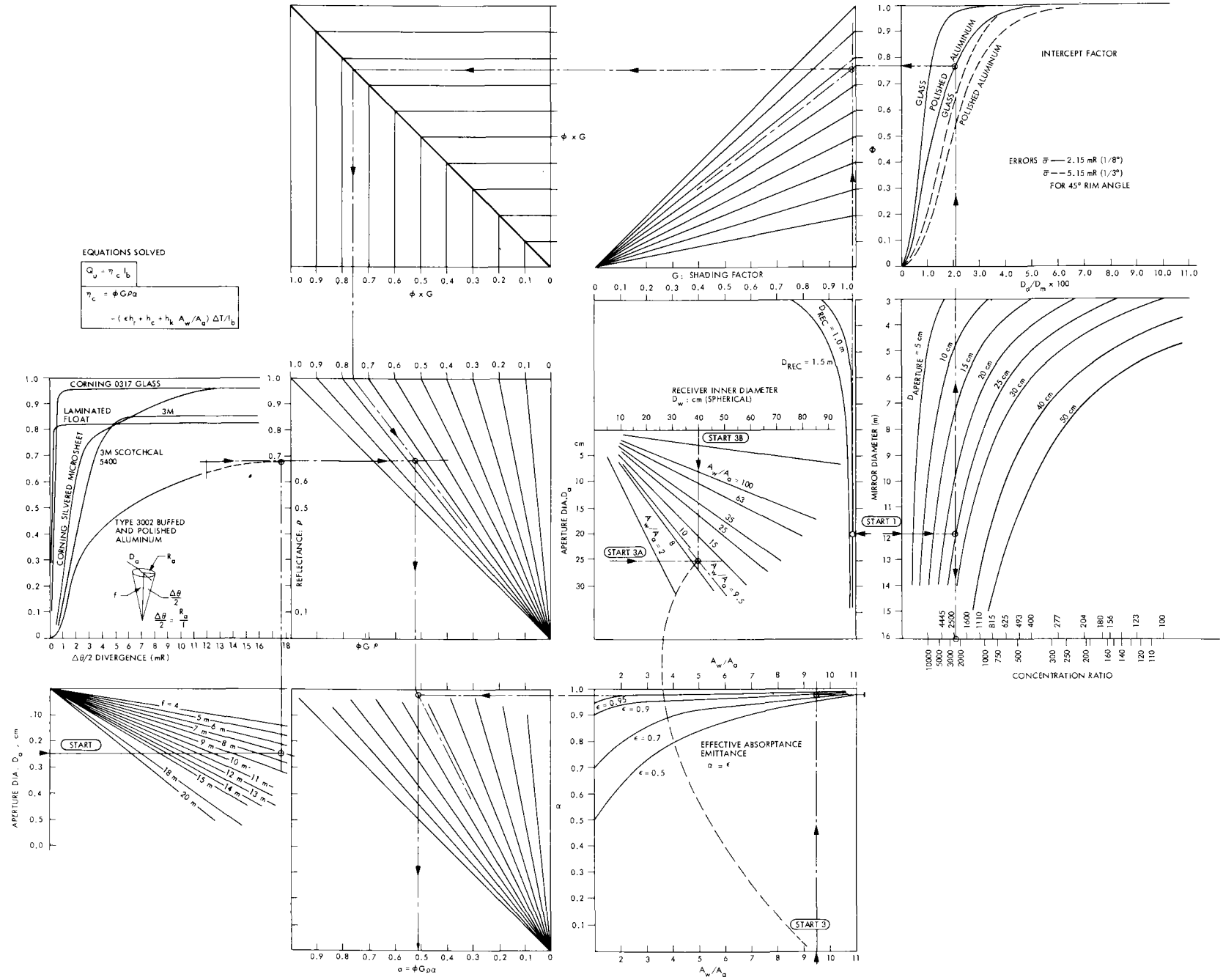

Figure A-2. Component A of the Nomogram that Gives the Net Absorptance, a, from $a = \phi G \rho \alpha$

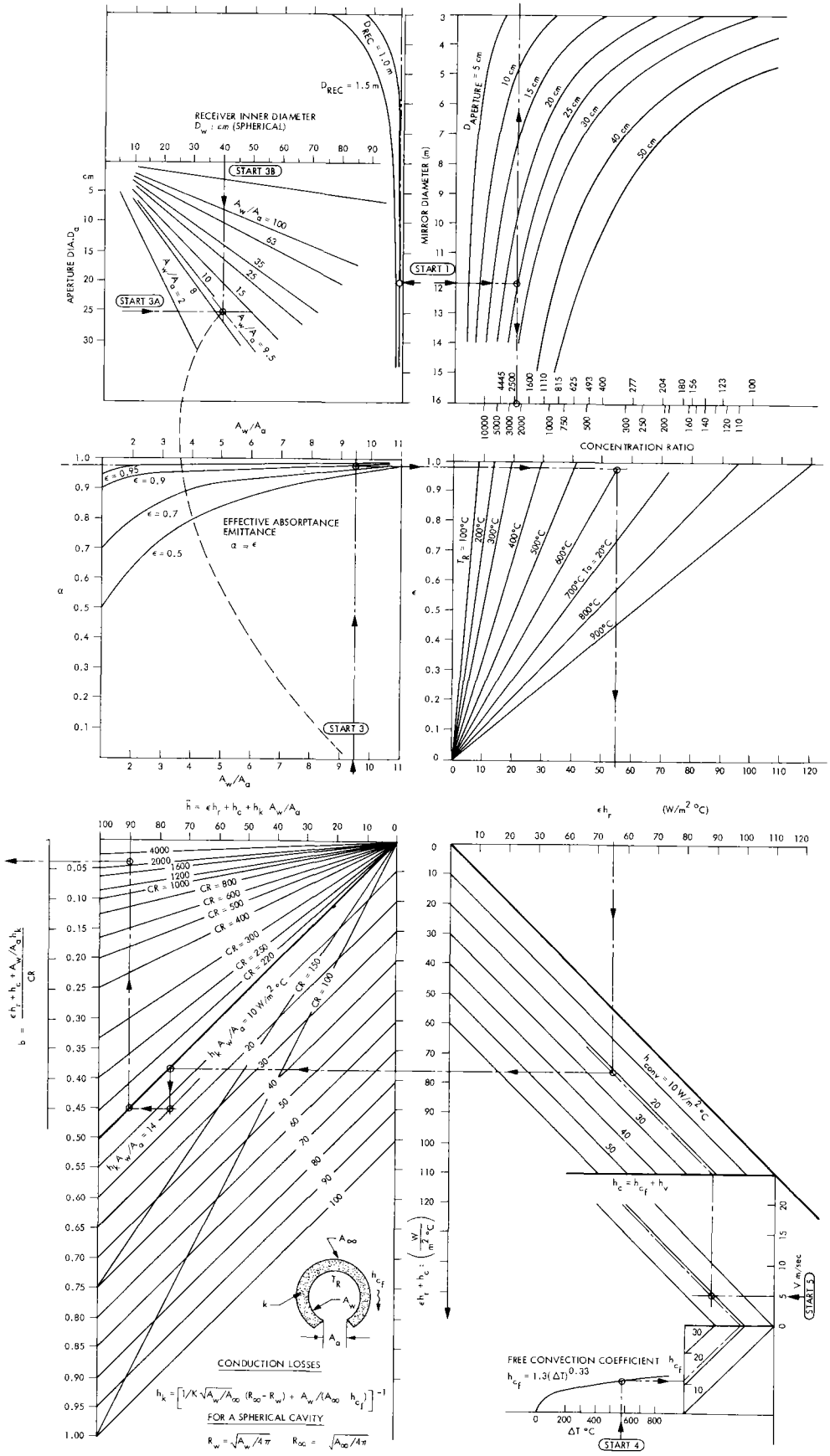

Figure A-3. Component B of the Nomogram that Gives the Heat Loss Coefficient, b, from $b = [\epsilon h_r + h_c (A_{rw}/A_a) h_k]/CR$

Enter Component B with the following inputs:

Receiver temperature, T_r = 600°C; k = 0.1 W/m °C; T_a = 20°C; CR = 2300; ΔT = 580°C; A_{rw}/A_∞ = 0.42; A_{rw}/A_a = 9.5; R_∞ = 0.3 m; wind speed, V = 5 m/s; R_{rw} = 0.2 m; insulation thickness = 0.1 m; A_∞ = 1.081 m^2.

Component B yields the heat loss coefficient, b, together with intermediate results:

h_c = 21 W/m^2 °C convection; h_r = 55 W/m^2 °C radiation loss coefficient.

Conduction losses are calculated from (h_k A_{rw}/A_a):

$$h_k = \left\{ \frac{1}{k}\sqrt{\frac{A_{rw}}{A_\infty}}\,(R_\infty - R_{rw}) + \frac{A_{rw}}{A}\,\frac{1}{h_c} \right\}^{-1} \quad \text{for a spherical cavity}$$

h_k (A_{rw}/A_a) = 1.45 x 9.5 = 14 W/m^2 °C, h = 55 + 21 + 14 = 90 W/m^2 °C

b = $\bar{h}$/CR = 0.039 W/m^2 °C, Collector Area Basis.